ORDER FOR SUPPLIES OR SERVICES

PAGE OF PAGES: 1 | 9

IMPORTANT: Mark all packages and papers with contract and/or order numbers.

1. DATE OF ORDER: 05/04/2015	2. CONTRACT NO. (If any): NRC-HQ-13-C-04-0022
3. ORDER NO.: NRC-HQ-60-15-T-0001	4. REQUISITION/REFERENCE NO.: RES-15-0106

5. ISSUING OFFICE (Address correspondence to):
US NRC - HQ
ACQUISITION MANAGEMENT DIVISION
MAIL STOP TWFN-5E03
ATTN ROB ROBINSON 301-415-0728
WASHINGTON DC 20555-0001

6. SHIP TO:
a. NAME OF CONSIGNEE: US NUCLEAR REGULATORY COMMISSION-
b. STREET ADDRESS: MAIL PROCESSING CENTER
4930 BOILING BROOK PARKWAY
c. CITY: ROCKVILLE | d. STATE: MD | e. ZIP CODE: 20852

7. TO: DANIELLE C EVANS
a. NAME OF CONTRACTOR: PURDUE UNIVERSITY
b. COMPANY NAME:
c. STREET ADDRESS: 460 NORTHWESTERN AVE RM 301
d. CITY: WEST LAFAYETTE | e. STATE: IN | f. ZIP CODE: 479072024

f. SHIP VIA:

8. TYPE OF ORDER
☐ a. PURCHASE
REFERENCE YOUR: revised proposal -4/27/15
Please furnish the following on the terms and conditions specified on both sides of this order and on the attached sheet, if any, including delivery as indicated.
☒ b. DELIVERY
Except for billing instructions on the reverse, this delivery order is subject to instructions contained on this side only of this form and is issued subject to the terms and conditions of the above-numbered contract.

9 ACCOUNTING AND APPROPRIATION DATA: See Schedule

10. REQUISITIONING OFFICE: OFF OF NUCLEAR REG RESEARCH

11. BUSINESS CLASSIFICATION (Check appropriate box(es))
☐ a. SMALL ☐ b. OTHER THAN SMALL ☐ c. DISADVANTAGED ☐ d. WOMEN-OWNED ☐ e. HUBZone
☐ f. SERVICE-DISABLED VETERAN-OWNED ☐ g. WOMEN-OWNED SMALL BUSINESS (WOSB) ELIGIBLE UNDER THE WOSB PROGRAM ☐ h. EDWOSB

12 F.O.B. POINT:

13. PLACE OF		14. GOVERNMENT B/L NO.	15. DELIVER TO F.O.B. POINT ON OR BEFORE (Date)	16. DISCOUNT TERMS
a. INSPECTION: Destination	b. ACCEPTANCE: Destination			

17. SCHEDULE (See reverse for Rejections)

ITEM NO. (a)	SUPPLIES OR SERVICES (b)	QUANTITY ORDERED (c)	UNIT (d)	UNIT PRICE (e)	AMOUNT (f)	QUANTITY ACCEPTED (g)
	The U.S. Nuclear Regulatory Commission issues this Task Order in support of the project entitled,"Post-CHF Heat Transfer at High Pressure and Flow Conditions: Experimental Support for TRACE Model Development" Continued ...					

SEE BILLING INSTRUCTIONS ON REVERSE

18. SHIPPING POINT:
19. GROSS SHIPPING WEIGHT:
20. INVOICE NO.:
17(h) TOTAL (Cont. pages): $888,680.00

21. MAIL INVOICE TO:
a. NAME: US NUCLEAR REGULATORY COMMISSION
b. STREET ADDRESS (or P.O. Box): ONE WHITE FLINT NORTH
11555 ROCKVILLE PIKE
MAILSTOP O3-E17A
NRCPAYMENTSNRCGOV
c. CITY: ROCKVILLE | d. STATE: MD | e. ZIP CODE: 20852-2738
17(i) GRAND TOTAL: $888,680.00

22. UNITED STATES OF AMERICA BY (Signature): 05/05/2015

23. NAME (Typed): SHARLENE M. MCCUBBIN
TITLE: CONTRACTING/ORDERING OFFICER

AUTHORIZED FOR LOCAL REPRODUCTION
PREVIOUS EDITION NOT USABLE

OPTIONAL FORM 347 (Rev. 2/2012)
Prescribed by GSA/FAR 48 CFR 53.213(f)

TEMPLATE - ADM001

SUNSI REVIEW COMPLETE MAY 07 2015 ADM002

IMPORTANT: Mark all packages and papers with contract and/or order numbers.

DATE OF ORDER	CONTRACT NO.	ORDER NO.
05/01/2015	NRC-HQ-13-C-04-0022	NRC-HQ-60-15-T-0001

ITEM NO. (a)	SUPPLIES/SERVICES (b)	QUANTITY ORDERED (c)	UNIT (d)	UNIT PRICE (e)	AMOUNT (f)	QUANTITY ACCEPTED (g)
	Period of Performance: 6/1/2015 - 5/31/2018 Total Task Order Ceiling: $888,680.00 Total Obligated Amount: $420,000.00 See attached pages for specifc details regarding this Task Order. Contractor Acceptance of Task Order: NRC-HQ-60-15-T-0001 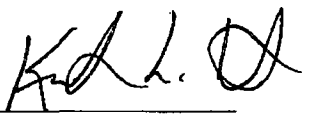 Signature MAY 04 2015 Date Kenneth W. Suter Contract Analyst Title Period of Performance: 06/01/2015 to 05/31/2018					
00001	Cost Line Item Ceiling$888,680.00 Incrementally Funded Amount: $420,000.00 Accounting Info: 2015-X0200-REIM-60-60D003-11-R-729-1302-252A Funded: $135,000.00 Accounting Info: 2015-X0200-FEEBASED-60-60D003-17-6-161-1061-252A Funded: $250,000.00 Accounting Info: 2015-X0200-FEEBASED-60-60D003-11-6-213-1045-252A Funded: $35,000.00 Continued ...				888,680.00	

TOTAL CARRIED FORWARD TO 1ST PAGE (ITEM 17(H)) $888,680.00

IMPORTANT: Mark all packages and papers with contract and/or order numbers.

DATE OF ORDER	CONTRACT NO.	ORDER NO.
05/04/2015	NRC-HQ-13-C-04-0022	NRC-HQ-60-15-T-0001

ITEM NO. (a)	SUPPLIES/SERVICES (b)	QUANTITY ORDERED (c)	UNIT (d)	UNIT PRICE (e)	AMOUNT (f)	QUANTITY ACCEPTED (g)
	The obligated amount of award: $420,000.00. The total for this award is shown in box 17(i).					

TOTAL CARRIED FORWARD TO 1ST PAGE (ITEM 17(H)) $0.00

A.1 NRCB010 BRIEF PROJECT TITLE AND WORK DESCRIPTION

(a) The title of this project is: Post-CHF Heat Transfer at High Pressure and Flow Conditions: Experimental Support for TRACE Model Development.

(b) Summary work description: The objective of the task order is to provide the experimental data necessary for the improvement of the TRACE models for inverted annular and inverted slug film boiling. The improvement of the models for these regimes was identified as a high priority near-term development need in the Thermal-Hydraulic Code Development Plan. This effort will also support the implementation of the droplet field into TRACE by determining the conditions at the onset of dispersed flow film boiling for reflood conditions. The incorporation of the droplet field is planned for the next major release of TRACE.

This objective will be realized by performing steady-state low-quality film boiling experiments in a tubular test section. A major component of this experimental program is the utilization of the X-ray radiography system being developed at the University of Michigan under Task Order #2 of the THI contract. This advanced two-phase instrumentation system will provide not only for the accurate measurement of the void fraction during post-CHF conditions but also provide information on the flow topology such as the size and shape of the liquid slugs in the ISFB regime.

The test procedures and instrumentation will be designed to provide the information necessary to develop the following models for both IAFB and ISFB:

- Wall heat transfer
- Interfacial friction
- Flow regime transition criteria

A.2 NRCB030A CONSIDERATION AND OBLIGATION—COST-REIMBURSEMENT – NO FEE ALTERNATE I

(a) The total estimated cost to the Government for full performance under this Task Order is **$888,680.00**.

(b) The amount presently obligated by the Government with respect to this Task Order is **$420,000.00**.

(c) It is estimated that the amount currently obligated will cover performance through May 2017.

(d) This is an incrementally-funded contract and FAR 52.232-22 – "Limitation of Funds" applies.

A.3 COST SCHEDULE

Period of Performance – 4/28/15 – 4/27/2018

Description	Total
Cost to Perform Requirements of the Task Order (Purdue)	$95,495
Cost to Perform Requirements of the Task Order (Subcontractor – Ohio State University)	$793,185
Grand Total	**$888,680.00**

A.4 NRCD020 BRANDING

The Contractor is required to use the statement below in any publications, presentations, articles, products, or materials funded under this contract/order, to the extent practical, in order to provide NRC with recognition for its involvement in and contribution to the project. If the work performed is funded entirely with NRC funds, then the contractor must acknowledge that information in its documentation/presentation.

Work Supported by the U.S. Nuclear Regulatory Commission (NRC), Office of Nuclear Regulatory Research, under Contract/order number NRC-HQ-13-C-04-0022 – NRC-HQ-60-14-T-0001.

A.5 NRCD010 PACKAGING AND MARKING

(a) The Contractor shall package material for shipment to the NRC in such a manner that will ensure acceptance by common carrier and safe delivery at destination. Containers and closures shall comply with the Surface Transportation Board, Uniform Freight Classification Rules, or regulations of other carriers as applicable to the mode of transportation.

(b) On the front of the package, the Contractor shall clearly identify the contract number under which the product is being provided.

(c) Additional packaging and/or marking requirements are as follows: N/A.

A.6 NRCF032 TASK/DELIVERY ORDER PERIOD OF PERFORMANCE (SEP 2013)

This order shall commence on Date of Award and will expire three years from the Date of Award.

A.7 NRCG030 ELECTRONIC PAYMENT (SEP 2014)

The Debt Collection Improvement Act of 1996 requires that all payments except IRS tax refunds be made by Electronic Funds Transfer. Payment shall be made in accordance with FAR 52.232-33, entitled "Payment by Electronic Funds-Central Contractor Registration".

To receive payment, the contractor shall prepare invoices in accordance with NRC's Billing Instructions. Claims shall be submitted on the payee's letterhead, invoice, or on the Government's Standard Form 1034, "Public Voucher for Purchases and Services Other than Personal," and Standard Form 1035, "Public Voucher for Purchases Other than Personal – Continuation Sheet." The preferred method of submitting invoices is electronically to: NRCPayments@nrc.gov.

A.8 NRCH480 USE OF AUTOMATED CLEARING HOUSE (ACH) ELECTRONIC PAYMENT/REMITTANCE ADDRESS

The Debt Collection Improvement Act of 1996 requires that all Federal payments except IRS tax refunds be made by Electronic Funds Transfer. It is the policy of the Nuclear Regulatory Commission to pay government vendors by the Automated Clearing House (ACH) electronic funds transfer payment system. Item 15C of the Standard Form 33 may be disregarded.

A.9 NRCH470 GREEN PURCHASING (SEP 2013)

(a) In furtherance of the sustainable acquisition goals included in Executive Order 13514, "Federal Leadership in Environmental, Energy, and Economic Performance," products and services acquired under this contract/order shall be energy-efficient (Energy Star or Federal Energy Management Program (FEMP) designated), water-efficient, biobased, environmentally preferable (e.g., Electronic Product Environmental Assessment Tool (EPEAT) certified), non-ozone depleting, recycled content, and non-toxic or less toxic alternatives, to the maximum extent practicable in meeting NRC contractual requirements.

(b) See NRC's Green Purchasing Plan (GPP) at: http://pbadupws.nrc.gov/docs/ML1219//ML12191A130.pdf and the General Service Administration's (GSA) Green Procurement Compilation at: http://www.gsa.gov/portal/content/198257.

(c) The contractor shall flow down this clause into all subcontracts and other agreements that relate to performance of this contract/order.

A.10 NRCH410 WHISTLEBLOWER PROTECTION FOR NRC CONTRACTOR AND SUBCONTRACTOR EMPLOYEES

(a) The U.S. Nuclear Regulatory Commission (NRC) contractor and its subcontractor are subject to the Whistleblower Employee Protection public law provisions as codified at 42 U.S.C. 5851. NRC contractor(s) and subcontractor(s) shall comply with the requirements of this Whistleblower Employee Protection law, and the implementing regulations of the NRC and the Department of Labor (DOL). See, for example, DOL Procedures on Handling Complaints at 29 C.F.R. Part 24 concerning the employer obligations, prohibited acts, DOL procedures and the requirement for prominent posting of notice of Employee Rights at Appendix A to Part 24 entitled: "Your Rights Under the Energy Reorganization Act".

(b) Under this Whistleblower Employee Protection law, as implemented by regulations, NRC contractor and subcontractor employees are protected from discharge, reprisal, threats, intimidation, coercion, blacklisting or other employment discrimination practices with respect to compensation, terms, conditions or privileges of their employment because the contractor or subcontractor employee(s) has provided notice to the employer, refused to engage in unlawful practices, assisted in proceedings or testified on activities concerning alleged violations of the Atomic Energy Act of 1954 (as amended) and the Energy Reorganization Act of 1974 (as amended).

(c) The contractor shall insert this or the substance of this clause in any subcontracts involving work performed under this contract.

A.11 NRCH340 COMPLIANCE WITH U.S. IMMIGRATION LAWS AND REGULATIONS

NRC contractors are responsible to ensure that their alien personnel are not in violation of United States immigration laws and regulations, including employment authorization documents and visa requirements. Each alien employee of the Contractor must be lawfully admitted for permanent residence as evidenced by Permanent Resident Form I-551 (Green Card), or must present other evidence from the U.S. Department of Homeland Security/U.S. Citizenship and Immigration Services that employment will not affect his/her immigration status. The U.S. Citizenship and Immigration Services provides information to contractors to help them understand the employment eligibility verification process for non-US citizens. This information can be found on their website, http://www.uscis.gov/portal/site/uscis.

The NRC reserves the right to deny or withdraw Contractor use or access to NRC facilities or its equipment/services, and/or take any number of contract administrative actions (e.g., disallow costs, terminate for cause) should the Contractor violate the Contractor's responsibility under this clause.

A.12 NRCH080 CONTRACTOR ACQUIRED GOVERNMENT EQUIPMENT/PROPERTY

(a) The Contractor is authorized to acquire and/or fabricate the equipment/property listed below for use in the performance of this contract.

1. Equipment categorized as "Capital Equipment" in the March 4, 2015 proposal submitted by Purdue University (on behalf of Ohio State University, the subcontractor).

(b) In the event that, during contract performance, the contractor determines that the acquisition cost for the above item(s) is expected to exceed the amount(s) contained in the contractor's proposal, the contractor shall refer to the Limitation of Cost or Funds Clause when either is included in the contract.

(c) Only the equipment/property listed above, in the quantities shown, will be acquired by the contractor unless the contractor receives written authorization and approval from the contracting officer for the purchase of additional equipment/property. The above listed

items are subject to FAR 52.245-1 – "Government Property".

A.13 LIST OF ATTACHMENTS

1. Task Order Statement of Work
2. Background Information for Task Order on Post-CHF Heat Transfer at High Pressure and Flow Conditions
3. Hot Patch Design Study

STATEMENT OF WORK

Post-CHF Heat Transfer at High Pressure and Flow Conditions: Experimental Support for TRACE Model Development

I. BACKGROUND

The USNRC's system thermal-hydraulic analysis code TRACE (TRAC RELAP Advanced Computational Engine) is being developed by the NRC to perform large and small break loss of coolant accident and system transient analyses for a wide range of nuclear plants. This code will be used as an audit tool to analyze transient and accident analyses submitted by the vendors and licensees. Two post-CHF flow regimes, inverted annular and inverted slug film boiling, are the focus of the task order. In particular, this task order will address these post-CHF regimes in a tubular test section with a stabilized quench front to allow for steady-state conditions and thereby facilitate model development. As explained below, this experimental program has been designed to complement that of the small rod bundle post-CHF experiments currently in the planning stages at Penn State as part of the spacer grid thermal-hydraulics program.

As described in attachment #1, the inverted annular film boiling (IAFB) regime occurs just downstream of the quench front and its precursory cooling largely governs the quench front progression by reducing the clad temperature to the point where surface rewetting can begin. In addition, its void fraction, due to its effect upon the downcomer-to-core gravity head, affects the core inlet flooding rate. Further downstream, the breakup of the inverted annular core gives rise to the inverted slug film boiling (ISFB) region that provides the initial condition for the dispersed flow regime where the peak clad temperature occurs. Therefore, for the accurate prediction of post-CHF clad temperatures in transients such as large and intermediate break loss of coolant accidents (LOCA), accurate models with quantified uncertainties are required for the calculation of both the wall heat transfer and the void fraction in these regimes.

High pressure IAFB can occur during an Anticipated Transient Without Scram (ATWS) event while regions of a BWR core exceed the critical heat flux during power oscillations. Both the IAFB and ISFB regimes can occur at high pressure in a PWR during the blowdown rewet phase of a large-break LOCA or during loop seal clearance with a partially uncovered core in a small-break LOCA. These scenarios involve high pressure post-CHF flow conditions for which very little data exists. Recently, some TRACE simulations have indicated that ATWS related oscillations may result in maximum cladding temperatures near the 2200 °F regulatory limit. Models in TRACE and most other thermal-hydraulic codes are largely based on low pressure data and then extrapolated. Thus, the possible bias and high uncertainty in these models is difficult to quantify and has complicated the review process. Accurate models with well-defined uncertainties for the IAFB and ISFB regimes are therefore needed to support NRR and NRO in both near-term and future licensing activities.

Two-fluid codes such as TRACE frequently use ad hoc models for wall and interfacial heat transfer as well as interfacial shear in the inverted annular and inverted slug film boiling flow regimes. Consequently, the modeling of these regimes was the subject of criticism during the TRACE peer review. Moreover, the current IAFB and ISFB models under-predict blowdown cooling in the LOFT L2-6 assessment during the time period

when the insurge of water into the bottom of the core quenches the fuel rods. Therefore the improvement of the models for these regimes was identified as a high priority near-term development need in the Thermal-Hydraulic Code Development Plan.

The experimental effort called for in this statement of work is specifically targeted to the improvement of the TRACE constitutive models for the inverted annular and inverted slug film boiling regimes. Also, the transition from the ISFB to the dispersed flow film boiling (DFFB) regime will be investigated. This transition is due to droplet entrainment and the resulting constitutive models will support the addition of the droplet field into TRACE for reflood conditions. The incorporation of the droplet field in TRACE was also identified as a high priority near-term development need in the Thermal-Hydraulic Code Development Plan and this experimental effort supports that task as well.

For the inverted annular film boiling regime, the primary correlating variable is the vapor film thickness as deduced from the void fraction. The wall heat transfer correlation developed for TRACE 5.0 uses a non-dimensional form of the vapor film thickness to account for the large effect of system pressure upon the wall heat transfer coefficient. This relationship is based on laminar flow theory and there is insufficient high pressure IAFB void fraction data to verify it. Indeed, it appears that the pressure effect embodied in the TRACE formulation is overly conservative for high pressure and high flow conditions.

Similarly, recent investigations have indicated that the liquid-side interfacial heat transfer coefficient may have a pronounced mass flux effect for values of the mass flux above about 1000 (kg/m^2s). The interfacial heat transfer rate into the subcooled liquid core in IAFB governs the vapor generation rate at the interface and hence affects the vapor film thickness and wall heat transfer. The TRACE model for this interfacial heat transfer is a simple constant value of the Nusselt no. and the lack of a mass flux effect could also lead to a conservative bias in the wall heat transfer. There is little film boiling data at high flow rates such as would occur during oscillations in a BWR ATWS event and void fraction measurements are virtually non-existent.

This task order addresses these data needs for wall heat transfer and void fraction measurements for the IAFB and ISFB post-CHF regimes for high pressure and high flow conditions. Specifically, steady-state experiments will be conducted in a tubular test section where the quench front has been stabilized by using a directly heated hot patch (see attachment #2). This experimental program has been designed to complement that of the small rod bundle post-CHF experiments currently in the planning stages at Penn State as part of the spacer grid thermal-hydraulics program. In particular:

- Overlap tests will be conducted to quantify the effect of the rod bundle geometry vis-à-vis that of a tubular test section,
- Experiments at high values of the pressure, mass flux and subcooling will be conducted to provide coverage where the transient rod bundle tests may be too rapid to allow for accurate measurement of subchannel averaged void fractions using the gamma-ray tomography system,
- A systematic variation of pressure will be used to modify the non-dimensional formula for the vapor film thickness so that pressure effects are correctly accounted for, and
- Tests at high mass flux conditions will be conducted to determine the magnitude of the mass flux effect upon the liquid-side interfacial heat transfer coefficient.

To elucidate the data needs for model development and to describe the previous experimental programs, attachment #1 has sections describing:

- Post-CHF flow regimes
- Two-fluid modeling of IAFB
- Two-fluid modeling of ISFB
- Previous experimental programs

This attachment was included to enhance the shared understanding of the task at hand and was used in developing the requirements detailed below.

II. OBJECTIVE

The objective of this task order is to provide the experimental data necessary for the improvement of the TRACE models for inverted annular and inverted slug film boiling. The improvement of the models for these regimes was identified as a high priority near-term development need in the Thermal-Hydraulic Code Development Plan. This effort will also support the implementation of the droplet field into TRACE by determining the conditions at the onset of dispersed flow film boiling for reflood conditions. The incorporation of the droplet field is planned for the next major release of TRACE.

This objective will be realized by performing steady-state low-quality film boiling experiments in a tubular test section. A major component of this experimental program is the utilization of the X-ray radiography system being developed at the University of Michigan under Task Order #2 of the THI contract. This advanced two-phase instrumentation system will provide not only for the accurate measurement of the void fraction during post-CHF conditions but also provide information on the flow topology such as the size and shape of the liquid slugs in the ISFB regime.

The test procedures and instrumentation will be designed to provide the information necessary to develop the following models for both IAFB and ISFB:

- Wall heat transfer
- Interfacial friction
- Flow regime transition criteria

III. WORK REQUIREMENTS

Before detailing the individual tasks, deliverables and milestones that will be required under this task order, a listing of specific requirements that the proposed experimental approach must satisfy are given below. These specific requirements are given in the form of a bulleted list and are organized into the following categories: testing, geometry, and instrumentation requirements.

Testing Requirements:

- Shall be capable of performing steady-state inverted annular and inverted slug film boiling experiments in upflow conditions.

- Shall provide for testing over a pressure range from 0.138 MPa [20 psia] to 3.5 MPa [500 psia] to provide suitable data to resolve pressure scaling questions. A higher pressure level, up to 7 MPa [1000 psia], would be preferable if attainable within the task order budget.
- Shall provide for a water flow rate such that the mass flux ranges from 150 to 2,000 (kg/m^2s).
- Shall provide for a parametric variation of inlet subcooling with values up to at least 50 °C.

Geometry Requirements:

- Shall consist of a joule-heated tube with an internal diameter in the range of that for the hydraulic diameter of BWR and PWR fuel assemblies.
- Shall have a heated length approximately equal to that of two grid spans in a prototypic PWR rod bundle, that is, about 1.0 m.
- Shall employ a directly heated "notch type" hot patch located near the lower end of the heated length capable of stabilizing the bottom quench front. See attachment #2 for a description of the notch type hot patch and the results of a design study.
    - Shall employ plate type electrodes to power the hot patch with a minimum thickness to minimize distortions of the heat flux profile in this region.
    - Shall minimize the axial spacing between the electrodes powering the hot patch so as to reduce the preheating of the working fluid.
    - Shall have thermocouples to measure the wall temperature of the "hot notch".
- Shall contain a hot patch located near the upper end of the heated length to prevent top-down quench front progression due to a liquid film on unheated portion of the tube.
- Shall include a flow development region below the bottom hot patch elevation with a length of at least 20 L/D's.
- The tubular test section shall be composed of a material that does not undergo significant oxidation at film boiling temperatures. Furthermore, the electrical resistivity of the selected material should have very low temperature dependence (e.g., similar to that of Inconel-600).

Instrumentation Requirements:

- Flow loop instrumentation shall be provided for the test section outlet pressure, inlet temperature and inlet flow rate.
- Power shall be measured for the heater rods and for every separately heated hot patch.

- Shall use a suitably designed automatic power control system for the bottom hot patch power based on temperature feedback from the hot patch thermocouples rather than manual adjustments.
- Thermocouples shall be provided to measure the surface temperature of the test section wall for at least fifteen axial elevations.
    - The axial spacing of these thermocouples should be arranged so as to provide finer resolution of the axial profile just downstream of the hot patch. For example, in the experiment of Fung (1981), the wall thermocouple elevations were located at z = 3, 6, 9, 12, 18, 24, 35, 45, 50, and 55 cm downstream of the hot patch.
- A fluid thermocouple shall be provided to measure the temperature of the subcooled liquid core in IAFB as near to the end of the heated length as possible (upstream is preferable).
    - It would be preferable to have a thermocouple probe that could perform an axial traverse along the tube centerline to measure the core liquid temperature. However, due to the uncertainty of sealing constraints for high pressure conditions, this is not a requirement.
- The pressure drop over the heated length shall be measured using a differential pressure cell with the taps located as close to the beginning and end of the heated length as possible.
- The test facility shall be constructed to allow for the use of the X-ray radiography system being developed by the University of Michigan under task order #2 of the THI contract. Specifically,
    - Consultation with the University of Michigan will be required to assure that the design of the test facility does not interfere with that of the advanced instrumentation system and allows for traversing the entire heated length.
    - Test section and insulation materials shall be chosen so as to minimize their impact on the X-ray radiography system.

Should any of the above requirements not be able to be met, the requirement may be waived if it can be demonstrated that the objectives of the experiment can still be met. The individual tasks, deliverables and milestones that will be required under this task order are given below.

Task 1: Flow Loop Design and Construction

The first element of this task is the design of the flow loop and the determination of its operating procedure for the film boiling experiments. A letter report describing the proposed flow loop, its operating procedure, and how the testing requirements given above will be met shall be provided. Upon approval by the NRC project manager, procurement activities and construction of the flow loop may proceed.

Deliverables	Level of Effort	Completion Date
Letter report describing the design and operating ranges of flow loop.	3 Staff Months	4 months after award
Construction of the flow loop.	8 Staff Months	8 months after NRC approval

It is expected that all capital equipment costs, including those of the test section, will be less than $300K.

Task 2: Test Section Fabrication and Hot Patch Testing

The contractor shall design and fabricate a joule heated tubular test section to meet the testing, geometry and instrumentation requirements stated above. This test section shall employ a directly heated hot patch of the "notch type" described in Attachment #2 to stabilize the quench front. A letter report detailing the design of the test section and its instrumentation shall be delivered to the NRC. Upon approval by the NRC project manager, procurement activities and fabrication of the test section may proceed.

Upon completion of the test section it shall be installed in the flow loop and shakedown testing performed. This shakedown testing program will include determining the correct control procedure for the hot patch power supply so as to stabilize the quench front. This testing program shall demonstrate correct operation of the hot patch over a wide range of flow conditions. In addition the test section heat loss as a function of wall temperature shall be characterized during these shakedown tests.

A technical review meeting shall be held to discuss the design of the test section, its instrumentation (including the operation of the X-ray radiography system), and the shakedown testing program.

Deliverables	Level of Effort	Completion Date
Letter report documenting test section design and instrumentation.	2 Staff Months	8 months after award
Technical review meeting.		8 months after award
Test section fabrication.	3 Staff Months	4 months after NRC approval
Hot patch shakedown testing.	3 Staff Months	8 months after NRC approval

Task 3: Advanced Instrumentation System

The objective of this task is the installation, and shakedown testing of the advanced instrumentation measurement system. This task would also account for the packing and shipping costs associated with moving the X-ray radiography system from the University of Michigan (should this task order be placed with a different THI member institution). Similarly, though the University of Michigan has been separately tasked to provide training materials for the instrument, any consulting costs necessary to insure its proper operation in the film boiling test facility shall be borne by the subcontractor for this task order.

Deliverables	Level of Effort	Completion Date
Installation and shakedown testing of X-ray radiography system in film boiling test facility.	2 Staff Months	2 months after completion of the hot patch shakedown testing

Task 4: Inverted Annular Film Boiling Test Series

The contractor shall conduct a series of steady-state film boiling tests in the film boiling test facility with subcooled inlet conditions targeted at the IAFB regime. The test matrix shall include at least six pressure levels and five inlet velocities. In particular, the test matrix shall include a series of tests designed to replicate the conditions of the high flooding rate reflood tests that were previously conducted in the RBHT facility. That is, pressures of 0.138 MPa [20 psia], 0.276 MPa [40 psia] and 0.414 MPa [60 psia] at a flooding rate of 15.24 cm/s [6 in/s]. Finally, if the test matrix for the planned small bundle post-CHF experiment is available at this time, a suitable subset of overlap tests will be conducted.

For each of these pressure, and inlet velocity combination, data scans at steady-state conditions for several different power levels should be performed as follows. First, steady film-boiling conditions should be established at the maximum test section power level consonant with the facility temperature limits; the power should then be reduced progressively in steps of about 10% with data scans taken at each power level until spontaneous collapse of the vapor film occurs. The conditions at the time of vapor film collapse will then be used to evaluate the minimum film boiling point.

In addition, the test matrix shall provide for a suitable number of repeat tests to demonstrate the repeatability of the results. The test matrix shall be proposed in a letter report and concurred upon by the NRC project manager. Data generated from these matrix tests shall be provided to the NRC in electronic format to facilitate model development. Specifically, a MS Excel workbook shall be provided with the data from each individual test comprising one worksheet. The format of these worksheets will be agreed to in consultations with the NRC project manager.

Deliverables	Level of Effort	Completion Date
Letter report documenting the proposed test matrix.	1/2 Staff Month	18 months after award
IAFB data to be provided in electronic format (see above).	6 Staff Months	27 months after award
Letter report documenting the IAFB test results.	1 Staff Month	28 months after award

Task 5: Inverted Slug Film Boiling Test Series

The contractor shall conduct a series of steady-state film boiling tests in the rod bundle test facility with subcooled inlet conditions targeted at the ISFB regime. The test matrix shall include at least six pressure levels and five inlet velocities. The test matrix and procedure shall be proposed in a letter report and concurred upon by the NRC project manager.

These ISFB experiments shall be conducted so as to expose the highest void measurement station to the full range of conditions for the ISFB region. That is, for a given value of the mass flux, the rod power and inlet subcooling would be adjusted to cause the transition from IAFB to ISFB to occur just upstream of the highest void measurement station. After a data scan was processed for those conditions, then the inlet subcooling would be reduced in steps causing the ISFB transition point to progress downwards into the test section thereby exposing the measurement station to progressively higher void fractions and vapor flows. This process would continue, with a data scan being recorded for each inlet subcooling step, until the operating point is reached where the flow regime at the test section exit transitioned to dispersed flow.

Data generated from these matrix tests shall be provided to the NRC in electronic format to facilitate model development as described above in Task #4.

Deliverables	Level of Effort	Completion Date
Letter report documenting the proposed test matrix.	1/2 Staff Month	27 months after award
ISFB data to be provided in electronic format.	6 Staff Months	36 months after award
Letter report documenting the IAFB test results.	1 Staff Month	36 months after award

Attachment #1: Background Information for Task Order on Post-CHF Heat Transfer at High Pressure and Flow Conditions

I. Introduction

The USNRC's system thermal-hydraulic analysis code TRACE (TRAC RELAP Advanced Computational Engine) is being developed by the NRC to perform large and small break loss of coolant accident and system transient analyses for a wide range of nuclear plants. This code will be used as an audit tool to analyze transient and accident analyses submitted by the vendors and licensees. As described below, the inverted annular film boiling (IAFB) regime occurs just downstream of the quench front and its precursory cooling largely governs the quench front progression by reducing the clad temperature to the point where surface rewetting can begin. In addition, its void fraction, due to its effect upon the downcomer-to-core gravity head, affects the core inlet flooding rate. Further downstream, the breakup of the inverted annular core gives rise to the inverted slug film boiling (ISFB) region that provides the initial condition for the dispersed flow regime where the peak clad temperature occurs. Therefore, for the accurate prediction of post-CHF clad temperatures in transients such as large and intermediate break loss of coolant accidents, accurate models with quantified uncertainties are required for the calculation of both the wall heat transfer and the void fraction in these regimes.

Two-fluid codes such as TRACE frequently use ad hoc models for wall and interfacial heat transfer as well as interfacial shear in the inverted annular and inverted slug film boiling flow regimes. Consequently, the modeling of these regimes was the subject of criticism during the TRACE peer review. Moreover, the current IAFB model under-predicts blowdown cooling in the LOFT L2-6 assessment during the time period when the insurge of water into the bottom of the core quenches the fuel rods. Therefore the improvement of the models for these regimes was identified as a high priority near-term development need in the Thermal-Hydraulic Code Development Plan. The experimental effort called for in this statement of work is specifically targeted to the improvement of the TRACE constitutive models for the inverted annular and inverted slug film boiling regimes.

Although much experimental work has been performed on inverted annular film boiling in the past, deficiencies exist in the presently available database that render it unsuitable for model development (though it can and will be used for the quantification of model uncertainties). Specifically, a consistent set of steady-state film boiling data is needed for prototypical rod bundle geometries with measurements of:

- Wall temperatures
- Void fractions
- Liquid-core temperatures

While almost all film boiling experiments report wall temperatures, the only data available for the inverted annular and inverted slug film boiling regimes in a rod bundle is that collected during reflood experiments which by their nature are transient. Although such transient data can be used in model development, significant uncertainties are introduced due to the quench front heat release rendering them more suitable for validation studies of the entire reflood model.

Since the introduction of the "hot patch" technique (Groeneveld 1974), a large database for film boiling in tubes has been developed. However, very little of this database includes the measurement of the void fraction and liquid-core temperature measurements are virtually non-existent. To elucidate the data needs alluded to above, brief descriptions of the post-CHF flow regimes, and the two-fluid modeling of the IAFB and the inverted slug film boiling (ISFB) regime are given below. These descriptions are then followed by a summary of the post-CHF experimental programs that were conducted in the previous THI contract.

II. Description of Post-CHF Flow Regimes

Before discussing the modeling needs, it helps to better characterize the regime itself, as there are several distinct flow regimes that may occur in film boiling. Based on the heat transfer characteristics observed in forced convection film boiling inside vertical tubes, Hammouda et al (1996) and El Nakla et al (2011) identified four distinct regimes as shown in Figure 1 for a case with a high value of the mass flux and for the refrigerant R-134a.

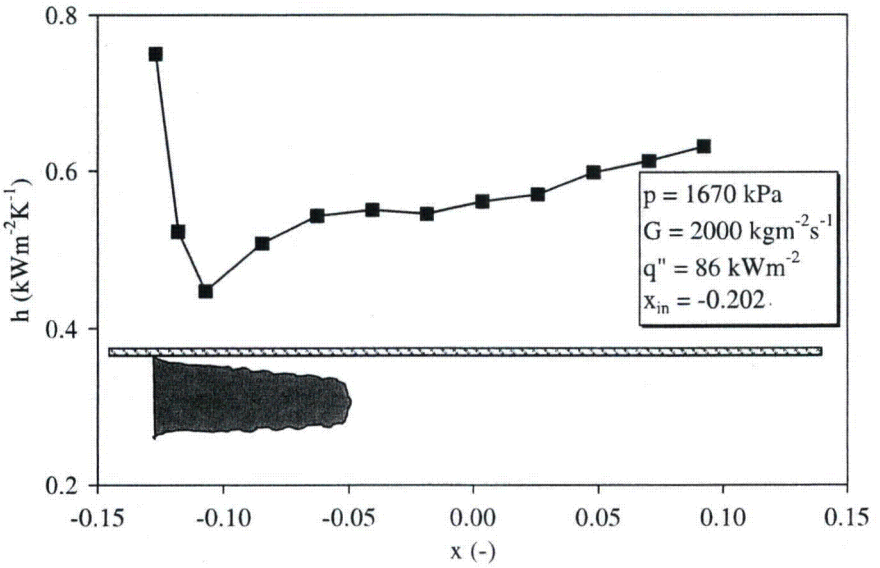

Figure 1: Heat transfer regimes during inverted annular film boiling (Nakla et al 2011).

Hammouda et al (1996) described these four regimes as:

- Region I: this region is usually referred to as the "subcooled IAFB" regime and is characterized by a strong decrease in the wall heat transfer coefficient in the direction of the flow as the subcooling of the liquid core is reduced and the vapor film begins to thicken. The vapor is confined to a thin layer at the superheated wall, the interface is smooth and stable, and significant non-equilibrium exists between the phases.

- Region II: further downstream, as the subcooling of the liquid core has been reduced due to interfacial heat transfer, the vapor velocity increases due to the increased vapor generation rate. In this region, the vapor layer thickness increases; the vapor-liquid interface becomes wavy and unstable; and convective heat transfer becomes important. This regime is generally accompanied by an increase in the wall heat transfer coefficient in the flow direction as the vapor flow increases and is referred to as the "wavy IAFB" regime.
- Region III: downstream of the wavy IAFB region, the flow regime might be that of "inverted slug flow" (ISF) or "agitated inverted annular flow" (AIAF). At low flow velocities, inverted slug flow is expected to be present: i.e. most of the liquid is in the form of liquid slugs in the center of the flow channel. At higher flow velocities, AIAF may be present; the liquid core may have a helical appearance or consist of sheet-like segments as a result of large amplitude roll waves. The flow is usually highly agitated and the vapor phase is distributed across the channel. Both ISF and AIAF represent transitions to the dispersed flow film-boiling region of region IV. In what follows, ISF will be used to denote both of these regimes.
- Region IV: the dispersed flow film-boiling (DFFB) regime occurs as the increasing vapor velocity induces breakup of the large liquid fragments of region III into droplets of various sizes. The wall heat transfer coefficient (referenced to the saturation temperature) may either increase or decrease in the flow direction as described below:
    - For high mass velocities, the vapor superheat is minimal, and an increase in quality results in an increase in vapor velocity and hence an increase in heat transfer coefficient.
    - For low mass velocities, convection also becomes more important as quality increases. However, reduced interfacial heat transfer to the droplets allows the vapor superheat to increase, so that the net effect is a decrease in the value of the effective wall heat transfer coefficient.

The focus of this task order is the subcooled and wavy inverted annular flow regimes (regions I and II) and the inverted slug flow regime (region III). In addition, the conditions at the onset of dispersed flow film boiling (region IV) will be determined.

III. Two-Fluid Modeling of IAFB

For a two-fluid model of IAFB, four types of constitutive models are needed:

- Wall heat transfer
- Interfacial friction
- Interfacial heat transfer
- Flow regime transition criteria (region II to III)

Each of these constitutive models is described in turn below together with the data needed for model development.

The heat transfer pathways present during IAFB are illustrated schematically in Figure 2 where:

- Qwv : wall-to-vapor heat transfer

- Qvi : vapor-to-interface heat transfer
- Qli : liquid-to-interface heat transfer
- Qrad : radiation heat transfer from wall-to-interface

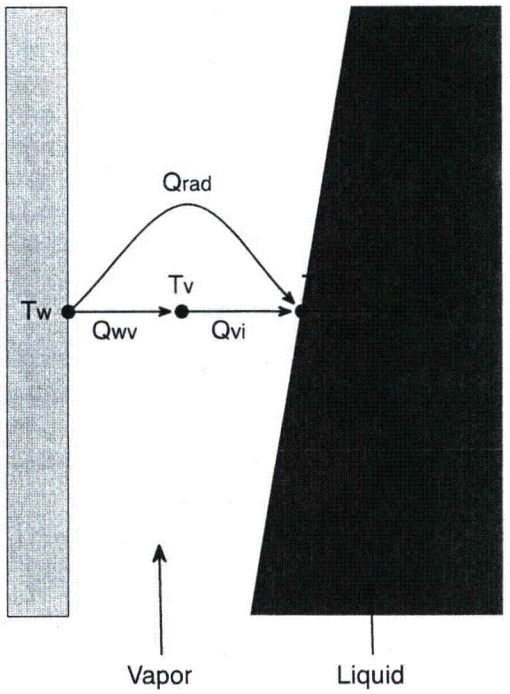

Figure 2: Heat transfer pathways for two-fluid model of IAFB.

The primary component of the wall heat transfer is convection from the wall to the vapor phase. Radiation heat transfer, from the wall to the liquid interface, occurs in parallel with the convective component but generally is of secondary importance and is not discussed here. It is customary to express the film boiling wall heat transfer convective component in terms of a heat transfer coefficient that is referenced to the saturation temperature as

$$h_w = \frac{\left(q''_w - q''_{rad}\right)}{\left(T_w - T_{sat}\right)} \qquad (1)$$

where

q''_w : total wall heat flux

q''_{rad} : wall heat flux due to radiation (estimated)

T_w : wall surface temperature

T_{sat} : saturation temperature

h_w : wall convective heat transfer coefficient

The wall-to-vapor heat transfer would then be given by

$$q''_{wv} = h_{wv}\left(T_w - T_v\right) = h_w\left(T_w - T_{sat}\right) \quad (2)$$

and the vapor-to-interface heat transfer by

$$q'_{vi} = h_{vi} \cdot P_i \cdot \left(T_v - T_{sat}\right) \leq h_w \cdot P_w \cdot \left(T_w - T_{sat}\right) \quad (3)$$

where P_i and P_w are the interfacial and wall perimeters respectively. The inequality in equation (3) results from the sensible heat that is absorbed by the vapor phase. Unfortunately, with respect to the needs for developing a two-fluid model of IAFB, all known empirical IAFB heat transfer correlations are of the type given by equation (1).

The reason for this simplified approach is the near impossibility of measuring the vapor temperature due to the thinness of the vapor film and the presence of interfacial waves on the liquid core. Consequently, some type of ad hoc formulation must be used to relate h_{wv} and h_{vi} to the overall wall heat transfer coefficient h_w. This is not a serious modeling deficiency and will not be addressed in this task order.

However, it is still necessary to develop a database sufficient for the development of a wall heat transfer model that is applicable to IAFB in rod bundles over a wide range of flow conditions. Initially, just downstream of the quench front, the vapor film is quite thin, the flow is laminar, the liquid is highly subcooled, and the vapor-liquid interface smooth. Under these conditions, almost all of the heat transferred from the wall to the interface is subsequently transferred into the liquid core as sensible heat resulting in little vapor generation. It is then appropriate to simply express the wall heat transfer coefficient as conduction across a vapor gap, that is,

$$h_w = \frac{k_v}{\delta} \quad (4)$$

where δ is the thickness of the vapor gap separating the wall from the liquid core and k_v is the vapor thermal conductivity. For such a laminar model, it is sufficient to measure the wall temperature (to get h_w) and the void fraction (to get δ). If possible, the direct measurement of the time-averaged vapor film thickness would be superior to that of the void fraction for this purpose.

Fung (1981) performed just such an experiment for steady state film boiling of water at atmospheric pressure in a tube using the hot patch technique. Figure 3 compares the film boiling heat transfer data of Fung to the laminar value given by equation (4) above. For void fractions less than about 10%, the laminar model represents the data quite well, however, as the void fraction increases a significant under-prediction becomes evident.

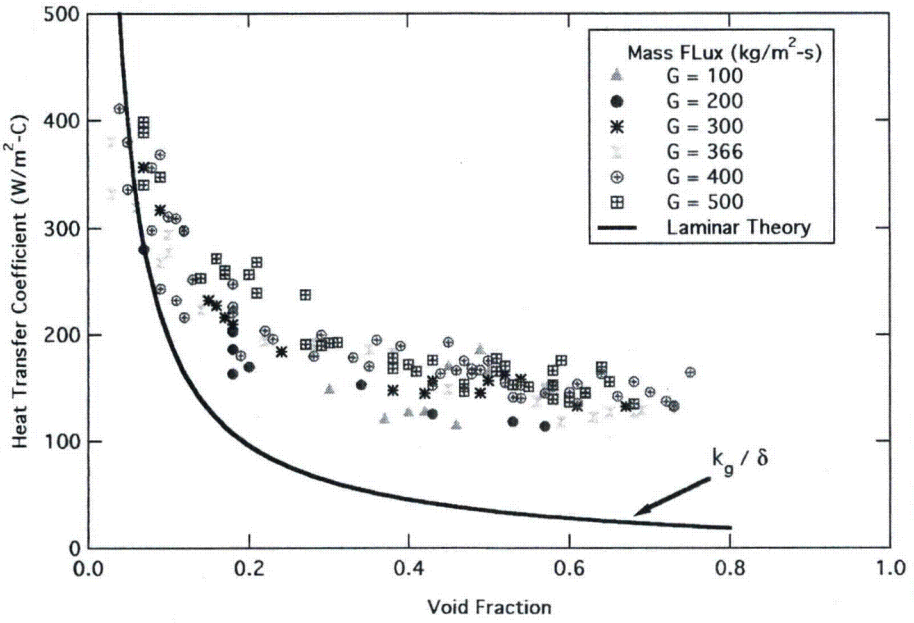

Figure 3: Comparison of Fung's low pressure IAFB data to laminar theory.

Further downstream, as the liquid-core subcooling decreases due to liquid-side interfacial heat transfer, the vapor generation rate increases and convective effects become more important. Two phenomena contribute to the enhanced wall heat transfer for this "wavy IAFB" regime:

- The effect of surface waves and/or oscillations of the liquid core upon the vapor heat transfer, and
- The possible transition of the vapor flow from the laminar to the turbulent regime.

De Cachard (1996) demonstrated that most of the enhancement due to the waviness of the vapor-liquid interface could be reasonably well correlated using a simple function of a non-dimensional vapor film thickness given by

$$\delta^* = \delta \cdot \left(\frac{\rho_v \cdot g \cdot \Delta\rho}{\mu_v^2} \right)^{1/3} \qquad (5)$$

This approach was used in the TRACE 5.0 model development and was successful in correlating IAFB data for both tubes (over a wide range of pressures) and rod bundles (for low pressure reflood conditions) though the heat transfer coefficient for rod bundles was enhanced about 30% above those for tubes. In subsequent code validation studies, this model was found to significantly under-predict the blowdown cooling in the LOFT L2-6 test during the time period when the insurge of water into the bottom of the core quenches the fuel rods. This under-prediction was attributed to the lack of modeling the turbulent flow effects on the vapor film heat transfer. For this reason, and to provide for a smoother transition to the inverted slug regime, the TRACE IAFB wall heat transfer model is proposed to be recast as both a function of the non-dimensional film thickness and the vapor Reynolds number. To accomplish this, a film boiling database is needed that includes information on the vapor mass flux in addition to both the wall temperatures

and void fractions. As discussed below, the estimation of the vapor mass flux from the equilibrium quality is not possible due to the substantial subcooling of the liquid core.

The void fraction, and hence the vapor-wall gap thickness, is governed primarily by the phasic flow rates and the interfacial friction. The pressure gradient term can be eliminated from the steady-state 1-D two-fluid momentum equations for IAFB to yield:

$$\tau_i = \frac{\alpha(1-\alpha)A}{P_i}\left\{\rho_l U_l \frac{dU_l}{dz} - \rho_v U_v \frac{dU_v}{dz} + g\cdot\Delta\rho + \frac{\tau_{wv}P_w}{\alpha A}\right\} \quad (6)$$

where

τ_i : interfacial shear stress (N/m^2)

τ_{wv} : wall-vapor phase shear stress (N/m^2)

For most IAFB conditions, the momentum flux terms are negligible in comparison to the buoyancy term; this allows equation (6) to be recast as

$$\alpha(1-\alpha)\cdot g\cdot\Delta\rho\cdot A \approx \tau_i\cdot P_i - (1-\alpha)\cdot\tau_{wv}\cdot P_w \quad (7)$$

Further, neglecting the wall-vapor shear stress[1] and substituting for the interfacial shear stress term gives

$$\alpha(1-\alpha)\cdot g\cdot\Delta\rho\cdot A \approx \tfrac{1}{2}\cdot\rho_v\cdot f_i\cdot P_i\cdot(U_v-U_l)^2 \quad (8)$$

and finally, in terms of the vapor mass flux, we have

$$\alpha(1-\alpha)\cdot g\cdot\Delta\rho\cdot A \approx \tfrac{1}{2}\cdot\rho_v\cdot f_i\cdot P_i\cdot\left(\frac{G_v}{\alpha\rho_v} - \frac{(G-G_v)}{(1-\alpha)\rho_l}\right)^2 \quad (9)$$

So, for an IAFB experiment where the void fraction is measured, the interfacial friction factor can be determined as long as the vapor mass flux is known.

Once again, to establish the values for the constitutive models needed for a two-fluid model of IAFB, we see that the crux of the matter is the determination of the vapor mass flux. As stated above, this determination is not a straightforward calculation employing the equilibrium quality, as would be done in a saturated two-phase experiment, due to the substantial subcooling of the liquid core in IAFB. Instead, the local value of the vapor mass flux has to be calculated by integration of the vapor mass equation

$$\frac{dG_v}{dz} = \Gamma_v \quad (10)$$

in the axial direction where Γ_v is the vapor generation rate per unit volume. Γ_v is given by an energy balance at the vapor-liquid interface, that is

$$\Gamma_v = \frac{q''_{rad}\cdot P_w + q''_{vi}\cdot P_i + q''_{li}\cdot P_i}{A(h_{v,sat}-h_l)} \quad (11)$$

[1] Note: in evaluating the interfacial friction factor from void fraction data, the wall shear stress term (and possibly the momentum flux terms) should not be neglected. These assumptions are made here solely for the purpose of clarifying the relationship between the void fraction, the interfacial friction and the phasic mass fluxes.

In equation (11), the usage of the subcooled liquid enthalpy, h_l, in the denominator accounts for the sensible heat required to raise the liquid from the subcooled liquid-core to the temperature of the interface.

Examining equation (11), we see that there are three heat fluxes that must be resolved so that the vapor mass flux can be determined. However, the first two of these can be related to the wall heat flux by performing an energy balance on the vapor film so that

$$\frac{q''_{wv} \cdot P_w - q''_{vi} \cdot P_i}{A} = G_v c_{P,v} \frac{dT_v}{dz} - \Gamma_v \left(h_v - h_{v,sat} \right) \tag{12}$$

yielding

$$\Gamma_v \cdot \left(h_v - h_l \right) = \frac{q''_w \cdot P_w + q''_{li} \cdot P_i}{A} - G_v \cdot c_{P,v} \cdot \frac{dT_v}{dz} \tag{13}$$

In equation (13), the two unknown heat fluxes, q''_{rad} and q''_{vi}, were eliminated but at the cost of adding two other unknowns: the superheated vapor enthalpy, h_v, and the axial gradient of the vapor temperature. Fortunately, suitable assumptions can be made to estimate these values without introducing a significant error. Specifically, the superheated vapor enthalpy can be evaluated by assuming that the vapor temperature is equal to the film temperature

$$T_v \approx \tfrac{1}{2}\left(T_w + T_{sat} \right) \tag{14}$$

and the vapor temperature gradient by

$$\frac{dT_v}{dz} \approx \frac{dT_w}{dz} \tag{15}$$

Therefore, in equation (13), there remains one significant unknown to be determined, namely the liquid-side interfacial heat transfer, q''_{li}. This interfacial heat flux is calculated from the liquid subcooling as

$$q''_{li} = h_{li} \cdot \left(T_l - T_{sat} \right) \tag{16}$$

where h_{li} is the liquid-side interfacial heat transfer coefficient.

There is almost no IAFB data available, either in tube or rod bundle geometries, from which even the magnitude of the liquid-side interfacial heat transfer coefficient can be estimated. As a result, all of the models proposed for this coefficient are ad hoc and subject to considerable uncertainty.

Consequently, the primary objective of this task order is to produce a database from which a reasonably accurate formulation for the liquid-side interfacial heat transfer coefficient can be deduced. With this formulation in hand, the vapor mass flux can be calculated so that a consistent set of constitutive models for both the wall heat transfer coefficient and the interfacial friction factor can be developed. Furthermore, it should be realized that for subcooled film boiling, it is this liquid-side interfacial heat transfer that governs the wall heat transfer. Basically, the effect is that the interfacial heat transfer determines the amount of vapor generation and hence controls the vapor film thickness, which in turn controls the wall heat transfer rate.

One way that the liquid-side interfacial heat transfer can be deduced is by measuring the axial gradient of the liquid temperature for the liquid core and then performing an energy balance over the liquid phase. Thence,

$$q''_{li} = G_l \cdot c_{P,l} \cdot \frac{dT_l}{dz} \tag{17}$$

In practice, one would not attempt to measure the actual liquid temperature gradient but rather approximate it from the difference between two measurement points, that is

$$\frac{dT_l}{dz} \approx \frac{\Delta T_l}{\Delta z} \tag{18}$$

Such an approach, where a centerline temperature measurement is used to approximate the bulk liquid temperature, should provide a reasonable estimate for the value of the liquid-side interfacial heat transfer while avoiding the attendant difficulties of measuring a heat flux at a vapor-liquid interface that is subject to surface waves and oscillatory motion.

The final constitutive model required to complete the two-fluid model for IAFB is the flow regime transition criteria from inverted annular (regions I and II) to inverted slug (region III). The general consensus is that this flow regime transition is associated with the breakup of the liquid core due to Kelvin-Helmholtz instability. It has also been observed that the point at which the breakup occurs is often close to the point at which the liquid core becomes saturated. This observation complements the Kelvin-Helmholtz theory in that the vapor flow rate rapidly increases as the liquid subcooling is lost and liquid-side interfacial heat transfer goes to zero.

Consequently, many authors have proposed that the breakup of the inverted annular core is governed by a critical Weber number,

$$We_{crit} = \frac{\rho_v \cdot \left(U_v - U_l\right)^2 \cdot D_c}{\sigma} = const \tag{19}$$

where D_c is the diameter of the liquid core and σ is the surface tension. Values suggested for this critical Weber number have ranged from 8 to 20 with no general consensus being reached. One of the problems in estimating the critical value of the Weber number, and indeed of applying this criterion, is that the interfacial drag model for IAFB must yield a calculated value for the Weber number that increases monotonically in the axial direction until breakup is predicted. For example, it is well known that as the vapor flow and film thickness increase that the magnitude of the interfacial friction factor increases markedly. If the proposed model for interfacial drag increases too rapidly as the vapor film thickens, then the product of the relative velocity and the liquid-core diameter may begin to decrease before the critical value of the Weber number is reached so that breakup is never predicted.

Consequently, the interfacial drag model and the flow regime transition criteria should be developed together in order to insure consistency. To provide a database from which a model for liquid core breakup can be developed, in addition to the measurements discussed above $\left(\alpha, T_w, T_l\right)$, the length of the inverted annular core also must be measured. The point at which core breakup occurs may be observed visually, for a test section with transparent walls or view ports, or possibly inferred from inflections in the

axial profiles of the other measured quantities. However, the transition from IAF to ISF appears to be very smooth so that it is difficult to identify inflection points in quantities such as the void fraction or wall heat transfer coefficient. Therefore, for this task order, it is preferable that some other means, such as visual observation or frequency analysis of fluid thermocouple or optical probe signals be used.

In summary, there are four constitutive models for which a database will be generated suitable for development of a consistent two-fluid model for IAFB:

- Wall heat transfer coefficient
- Interfacial friction factor
- Liquid-side interfacial heat transfer coefficient
- Flow regime transition criterion

To accomplish this task, the database shall include measurements for the axial profiles of the wall temperature, the void fraction, and the liquid core temperature. In addition, the breakup location of the inverted annular core will be required to be measured. If a suitable alternative method for determining the liquid-side interfacial heat transfer is proposed, then the measurement of the liquid core temperature can be omitted.

IV. Two-Fluid Modeling of ISFB

Typically, when subcooled liquid flows past the quench front, the flow regime is inverted annular and, just downstream of the quench front, a thin vapor film separates this subcooled liquid core from the superheated wall. The vapor velocity is low so that the flow is laminar and the vapor-liquid interface is smooth. Further downstream of the quench front, as the subcooling of the liquid core is reduced, the vapor flow increases causing the interface to first become wavy and then oscillate violently until breakup occurs at about the point where the liquid becomes saturated. Experimental data indicate that the inverted annular regime persists up to void fractions of 60-70% and that a smooth transition is made to the dispersed flow regime. This transitional regime will be denoted as inverted slug flow (ISF).

The ISF regime is considered to be composed of a mixture of large liquid chunks (i.e., liquid slugs resulting from the disintegration of the IAFB liquid core) and entrained droplets as depicted schematically in Figure 4. As the vapor flow increases, the liquid slugs are progressively broken up into smaller fragments and the fraction of the flow consisting of entrained droplets increases. Finally, the vapor velocity increases to the point where all of the liquid flow can be construed as entrained droplets and the regime is denoted as dispersed flow film boiling (DFFB). The key feature of the ISFB regime is that, with respect to the wall heat transfer, a smooth transition is provided from IAFB to DFFB.

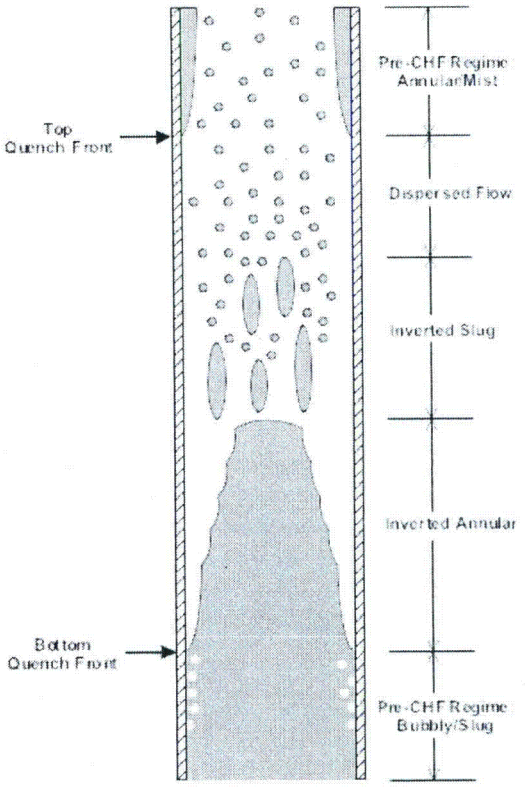

Figure 4: Schematic of the inverted flow regimes that occur for post-CHF conditions.

As no suitable models for the ISFB regime were available, TRACE 5.0 models this regime by using an ad hoc interpolation between IAFB and DFFB. Although the primary focus of this task order is the IAFB regime, a task to develop a database suitable for model development (or at least validation) of a model for ISFB is included. Consequently, the design of the flow loop, test section, and instrumentation must consider the data needs for ISFB.

To form a consistent set of models for the ISFB regime, the following constitutive models will need to be developed:

- Wall-to-vapor heat transfer
- Vapor-to-interface heat transfer
- Interfacial friction
- Wall-to-vapor shear
- Entrainment rate (or fraction)

A brief description of the data needs for each of these models follows.

The wall heat transfer mode is primarily that of turbulent forced convection to the vapor. The form of the model would probably be something similar to

$$q''_{wv} = \Psi_{2\Phi} \cdot h_{spv} \cdot \left(T_w - T_v\right) \tag{20}$$

where h_{spv} is the single-phase vapor heat transfer coefficient and $\Psi_{2\Phi}$ a "two-phase multiplier" to account for the enhancement effects due to the presence of the liquid chunks and droplets within the superheated vapor. The single-phase vapor heat transfer coefficient would be expected to be a function of the vapor Reynolds number and hence of the vapor mass flow rate. While the determination of the vapor flow rate was a critical factor for the IAFB models described above, it is not so much of a problem here. The reason is that the liquid phase can be considered to be saturated and hence, for a steady-state experiment, a good estimate of the vapor flow can be made from a simple energy balance. The two-phase enhancement factor is expected to be a function of the liquid loading and would require the measurement of the void fraction in addition to that of the wall temperature.

The wall heat transfer model given in equation (20) also relies upon the knowledge of the superheated vapor temperature. To a first approximation, the vapor temperature can be viewed as the result of two competing processes: wall heat transfer adding heat to the vapor, and interfacial heat transfer serving to cool the vapor by transferring heat to the liquid phase. For the sake of simplifying the discussion, we'll omit the other terms that would appear in an energy balance for the vapor phase and write

$$\frac{4}{D} \cdot \Psi_{2\Phi} \cdot h_{spv} \cdot \left(T_w - T_v\right) \approx h_{vi} \cdot A_i \cdot \left(T_v - T_{sat}\right) \tag{21}$$

Equation (21) then highlights the importance of the vapor-side interfacial heat transfer in determining the superheated vapor temperature. Unfortunately, due to the high liquid loadings in this regime, it is not practical to directly measure the vapor temperature due to thermocouple wetting and hence the interfacial heat transfer rate cannot be determined. Instead, models for the wall convective heat transfer and the vapor-side interfacial heat transfer will have to be developed together to provide a consistent modeling approach. Of course, any information that could be provided on the interfacial area or particle sizes for the ISF regime would significantly aid the model development effort and decrease the reliance on ad hoc assumptions.

To be consistent with the three-field model that will be part of the next major release of TRACE, the vapor-side interfacial heat transfer would be expressed as the sum of the contributions from the inverted slugs and the dispersed droplets. Then,

$$h_{vi} \cdot A_i = \left(h_{vi} \cdot A_i\right)_{IS} + \left(h_{vi} \cdot A_i\right)_{DF} \tag{22}$$

where the subscripts "*IS*" and "*DF*" refer to inverted slug and dispersed flow respectively. This type of formulation would provide a natural transition from the ISFB regime to DFFB as the fraction of the liquid phase treated as slugs would go to zero as the entrainment fraction approached unity. Of course, this places yet another data need on the modeling effort, namely the need to know the entrainment rate (or fraction).

The interfacial friction factor for ISFB[2] can be determined from equation (6) above more

[2] In a three-field model, the interfacial friction for the droplet field would be handled separately. As the volume fraction of entrained droplets would be miniscule (on the order of 0.005) it is not necessary to consider it in evaluating the interfacial shear for the inverted slugs.

simply than was the case for IAFB because good estimates for the phasic flow rates can be determined from a mass and energy balance. Thus, the sole data requirements are the measurements of the void fraction and pressure drop. For IAFB, it is customary to estimate the void fraction from a delta-P measurement by ignoring the momentum flux and wall shear, that is

$$\left[\alpha\rho_v + (1-\alpha)\rho_l\right]\cdot g\cdot\Delta z \;\approx\; \Delta P_{meas} \tag{23}$$

This approach is not acceptable for the ISF regime because the wall shear term is non-negligible. Therefore, an alternative measurement technique for the void fraction must be provided as discussed below.

The wall friction in the ISF regime would be correlated similar to that of the wall-to-vapor heat transfer using a suitable two-phase multiplier. That is, the pressure gradient due to wall-to-vapor drag would be expressed as

$$\left[\frac{dP}{dz}\right]_{frict} = \Phi_v^2\cdot\frac{2}{D_h}\cdot f_v\cdot\frac{G_v^2}{\rho_v} \tag{24}$$

Once again, the sole data requirements are the measurements of the void fraction and pressure drop as a good estimate of the vapor mass flux can be obtained from a mass and energy balance. Note that the temperature of the superheated vapor is needed in order to evaluate both the vapor density that appears explicitly in equation (24), and the viscosity that is implicit in the evaluation of the friction factor due to its Reynolds number dependence. As it is likely impractical to measure the vapor temperature, the value used here must be consistent with that resulting from the wall and interfacial heat transfer relations discussed above.

For the inverted annular flow regime, it is necessary to measure the axial evolution of the void fraction profile due to the wall heat transfer's strong dependence upon the vapor film thickness. These void fraction measurements must be either bundle average values or subchannel average values as point values would give no information on the vapor film thickness nor be suitable for model validation studies. As the frictional pressure drop in IAFB is relatively small compared to the buoyancy force, it is acceptable to infer the void fraction from differential pressure measurements. However, as noted above, the use of delta-Ps to infer void fraction is not acceptable for the inverted slug regime and hence an alternative measurement technique is required.

Traditionally, one would use a gamma densitometer to measure bundle average void fractions. In addition to the high costs associated with such a device, for a rod bundle employing heater rods composed of metal, the gamma source has to be quite strong. This may impose restrictions on the working environment, e.g. shielding, that would render this approach impractical.

The other constraints on the void measurement system are that it be non-intrusive and have a reasonable sampling time. The non-intrusive constraint arises from the desire not to perturb the flow regime for all the downstream locations, e.g. causing additional breakup of the liquid slugs. However, as was the case for traversing fluid thermocouples, an intrusive type probe may be used as long as it can be withdrawn from the test section flow area during a test or, as discussed below, only be used near the end of the heated length. The sampling rate constraint arises from the amount of time that would be required to hold the steady-state film boiling conditions constant to gather the data for one test. For example, if one were using an instrument such as an optical

probe to measure the time-averaged void fraction at one point in a subchannel, and then had to measure a sufficiently large enough number of points to be able to calculate a subchannel average value, it may not be possible to hold constant film boiling conditions long enough for such a measurement.

A possible alternative would be to use an intrusive void measurement system, such as a wire grid [see Manera et al (2009) and Arai et al (2012)], and locate it near the end of the heated length. The ISF experiments would then be conducted so as to expose this measurement station to the full range of conditions for the ISFB region. For example, for a given value of the mass flux, the rod power and inlet subcooling would be adjusted to cause the transition from IAFB to ISFB to occur just upstream of the void measurement station. After a data scan was processed for those conditions, then the inlet subcooling would be reduced in steps causing the ISFB transition point to progress downwards into the test section and exposing the measurement station to progressively higher void fractions and vapor flows. Eventually, the operating point would be reached where the flow regime at the bundle exit transitioned to dispersed flow. The entire range of conditions for ISFB could thus be covered using only one void measurement station. Additionally, the use of such advanced instrumentation might provide data on the interfacial area and geometry of the liquid slugs that would greatly aid model development.

With measurements of the wall temperature, the void fraction, and the pressure drop, a consistent set of model for the wall and interfacial heat transfer, the interfacial friction, and the wall drag could be developed. A limitation would be that the temperature of the superheated vapor calculated using this set of models could not be directly validated due to the impracticality of measuring the vapor temperature in the ISF regime. However, the overall performance of the model, and in particular its accuracy in predicting the rod surface temperature, could be quantified.

To predict the transition from ISF to dispersed flow, the entrainment rate or entrained fraction needs to be known. As was the case with the vapor temperature, it would be practically impossible to measure this in the inverted slug regime as it would require the ability to discriminate between flowing droplets and liquid chunks over a void fraction range of 60-90%. However, using a procedure such as described above to allow measurement of the void fraction at the bundle exit, one should be able to identify the point at which the flow has fully transitioned to dispersed flow. For these conditions then, one would know that the entrained fraction was unity. This would at least allow the development of a model that correctly predicted the point at which full entrainment occurred. Furthermore, for dispersed flow conditions, it would also be possible to measure the vapor superheat and possibly the droplet diameter. Knowing these parameters at the onset of the DFFB regime would then allow for more accurate modeling of that regime which is where the peak clad temperature occurs in a reflood transient.

In summary, the measurement of the wall temperature and pressure drop along the test section, and the void fraction and vapor temperature at the bundle exit, together with an experimental approach such as described above would enable the development of a consistent set of models for the inverted slug regime. These models would then replace the ad hoc interpolation scheme used in TRACE 5.0 and be consistent with the three-field model that will be used in its next major release. Further enhancements to the phenomenological bases of these models would accrue if measurement techniques were available to quantify the interfacial area for inverted slug flow and the droplet diameter at the onset of the dispersed flow regime.

V. Previous Experimental Programs

In the previous Thermal Hydraulic Institute program, there was a task order entitled "Post-CHF Heat Transfer and Hydrodynamics." A brief description of the experiments conducted under the auspices of this task order is given below. This statement of work is designed to build on the progress made during these previous efforts.

V.1. UCLA Vertical Plate Experiment

This experiment was conducted to investigate both the effects of mass flux and liquid subcooling upon the wall heat transfer coefficient in inverted annular film boiling. In addition, a unique feature of this experimental program was an effort to measure the liquid-side interfacial heat transfer rate. It is the effort that will be the focus of the discussion below. This experimental program is documented in Meduri's Ph.D. thesis (Meduri, 2007) and two papers (Meduri et al, 2006 and 2009).

Meduri's subcooled flow film boiling experiments were conducted using water at atmospheric pressure in a vertical flow channel with the heated surface being a vertical flat plate. The flow channel is depicted in Figure 5 and has a rectangular cross-section with one wall (labeled copper block) being heated. The heated surface was a temperature-controlled flat plate, 30.5 cm in height, and 3.175 cm wide. Data were obtained for mass fluxes ranging from 0 to 700 (kg/m^{2}s), inlet subcoolings ranging from 0 to 25 °C and wall superheats ranging from 200 to 400 °C.

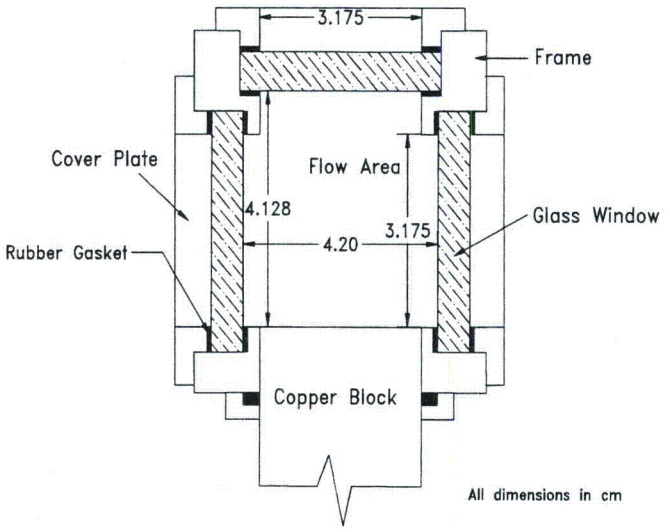

Figure 5: Cross-section of vertical flow channel used in UCLA flat plate experiments.

The unique feature of this experiment was the effort made to measure the liquid-side interfacial heat transfer coefficient. This was accomplished by using traversing micro-

thermocouples (see Figure 6) to measure the liquid temperature profile in the direction normal to the vapor-liquid interface. Some typical results are given in Figure 7 for three different subcoolings with a mass flux of 350 (kg/m^2s) and a wall superheat of 270 °C. In this figure, the horizontal line at 100 °C denotes the saturation temperature and hence the approximate location of the vapor-liquid interface.

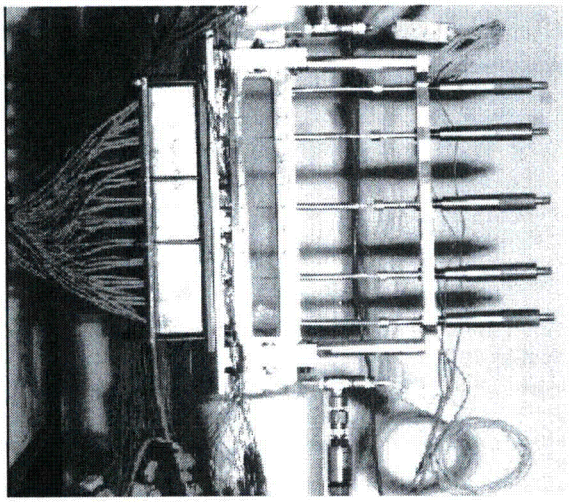

Figure 6: Side view of test section showing traversing micro-thermocouples.

Figure 7: Close-up view of typical time-averaged measurements of the liquid temperature profile near the vapor-liquid interface.

The liquid-side temperature gradient was estimated by calculating the gradient at the

vapor–liquid interface of a smooth profile (cubic polynomial) drawn through the measured liquid temperatures. Liquid-side interfacial heat fluxes were then estimated as

$$q''_{li} \approx k_l \left.\frac{dT_l}{dy}\right|_i \tag{25}$$

There are two questionable aspects of this experimental procedure. The first has to do with the nature of the interface itself as depicted in the photographs of Figure 8. Large interfacial waves would periodically wash over and then uncover the thermocouples obscuring not only the location of the interface but also affecting the time-averaged value of the temperature measurement in a somewhat unpredictable way. Secondly, equation (25) is only valid if the temperature gradient is indeed at the interface and within the laminar sublayer. For example, if the measured temperature gradient extended into the turbulent region, then the molecular thermal conductivity in equation (25) would need to be replaced by the turbulent thermal conductivity. Despite these reservations, the reported values for the liquid-side interfacial heat flux appear very reasonable. Their magnitude ranges from 60-100% of the wall heat flux and has the correct trends (e.g., increasing with liquid subcooling).

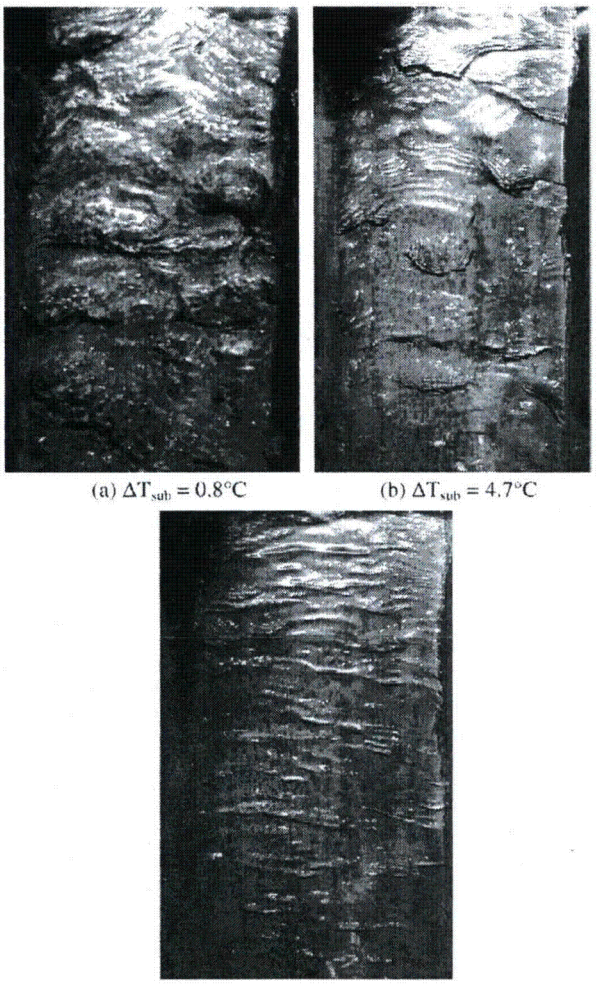

Figure 8: Visual observations showing interfacial waves for G = 350 (kg/m^{2}s), ΔTw = 250 °C, and (a) ΔTsub = 0.8 °C, (b) ΔTsub = 4.7 °C, and (c) ΔTsub = 9.5 °C.

Figure 9 gives a sampling of the results for the liquid-side interfacial heat transfer coefficient for a fixed wall superheat and subcooling[3] with mass flux as a parameter. Two surprising observations can be made from this figure. First, although there is a dependence upon the mass flux, it is relatively feeble. Comparing the results for a mass flux of 175 versus those for 750 (kg/m^{2}s), we see that the interfacial heat transfer coefficient only increases by about 30% while the mass flux has increased by a factor of four. This would imply a dependence upon the liquid Reynolds number to only about the 0.2 power instead of about 0.8 as would be expected for turbulent flow. Secondly, there is little apparent entrance length effect upon the interfacial heat transfer coefficient as

[3] Because of the large flow area used in these experiments, the liquid subcooling remained at essentially the inlet value over the entire length of the test section.

well. It should also be noted that the observations for this sampling of the results are also true for the entire set of data.

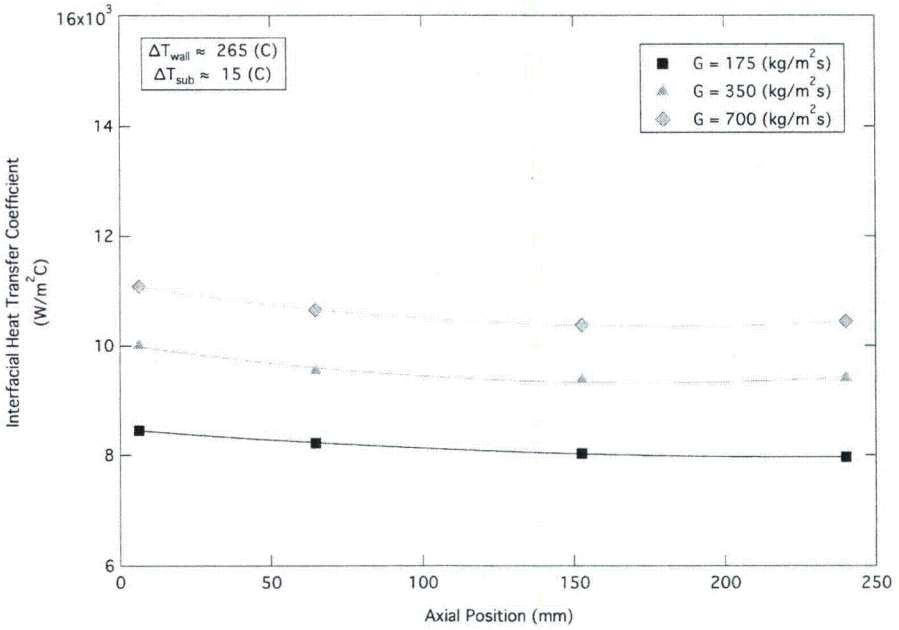

Figure 9: Effect of mass flux on the liquid-side interfacial heat transfer coefficient.

Figure 10 gives a sampling of the results for the liquid-side interfacial heat transfer coefficient for a fixed wall superheat and mass flux with subcooling as a parameter. Once again, a very surprising feature is noted. Namely the large increase in the magnitude of the interfacial heat transfer coefficient as the subcooling is reduced. This behavior would appear to be related to the changes in the structure of the vapor-liquid interface as depicted in Figure 8. Basically, when the liquid is significantly subcooled (see Figure 8c), the vapor film is thin, the vapor flow rate is low, and the surface is relatively smooth. As the subcooling decreases, see Figure 8b & c) the vapor flow increases, the vapor film thickens and large waves develop on the interface. I is supposed that the resultant surface oscillations promote mixing in the liquid core thereby enhancing the interfacial heat transfer.

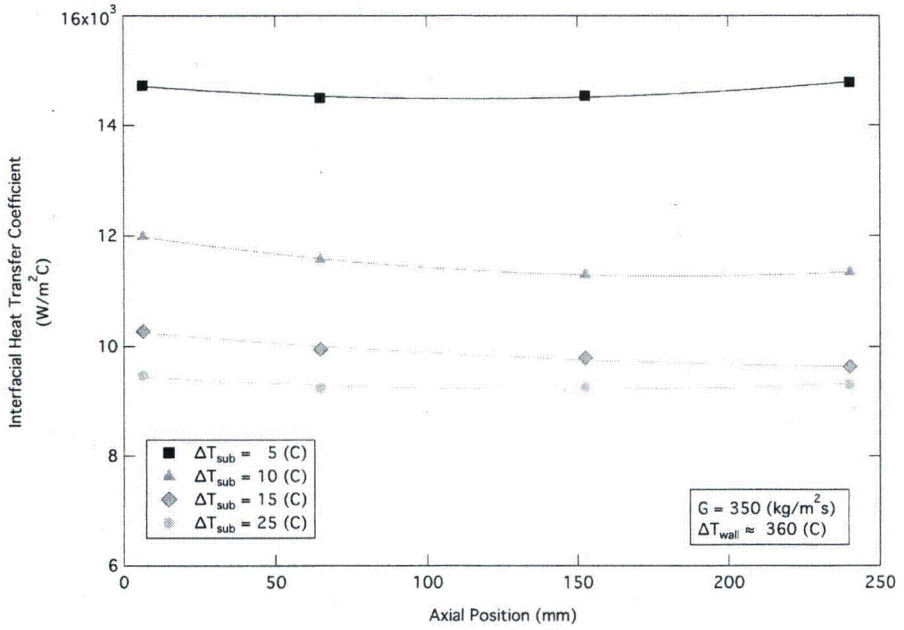

Figure 10: Effect of subcooling on the liquid-side interfacial heat transfer coefficient.

Figure 11 plots all of the liquid-side interfacial heat transfer coefficients that were inferred from the UCLA vertical plate experiment versus liquid subcooling with mass flux as a parameter. As noted above, there is a dependence upon mass flux, however, it is overshadowed by the subcooling effect. One other feature of the subcooling effect evident in Figure 11, see the data for a mass flux of 350 (kg/m^2s), is that it dies out for subcoolings greater than about 15 °C. Determining the dependence of the liquid-side interfacial heat transfer coefficient upon mass flux and its apparent dependence upon subcooling for IAFB in a rod bundle geometry will be a focus of this new task order.

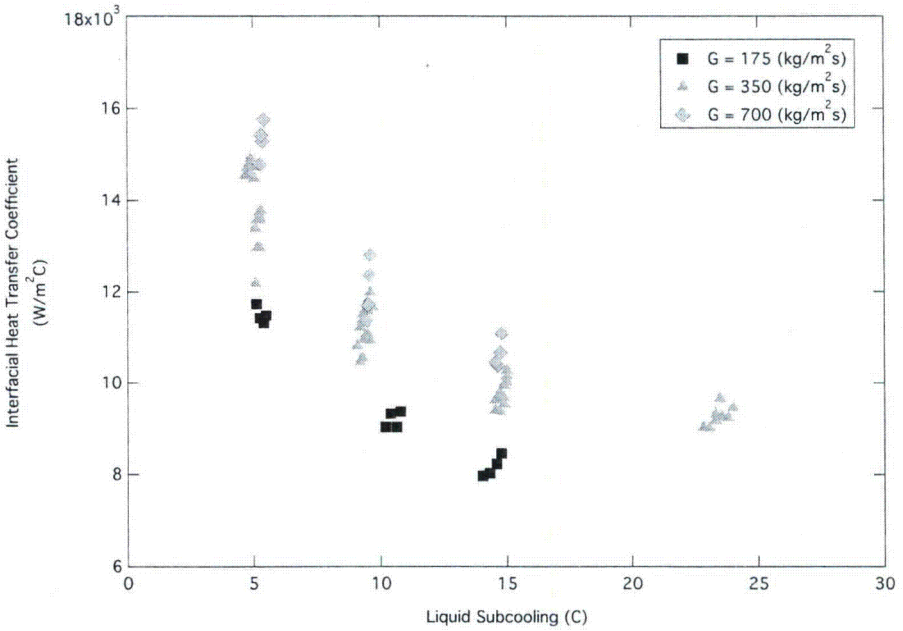

Figure 11: Inferred values of the liquid-side interfacial heat transfer coefficient versus subcooling with mass flux as a parameter.

Despite the interesting results presented above, there are several non-prototypical features of their experiment, as compared to the reflooding of a rod bundle, that prevent its direct use in the development of a model for TRACE. Specifically:

1. In this experiment, due to the large flow area (relative to the heated perimeter), the liquid temperature was essentially isothermal rather than increasing in the direction of the flow. Consequently, the liquid-side heat transfer and hence the vapor generation rate would stay approximately constant along the heated surface. Whereas in the real situation, the liquid subcooling decreases in the axial direction leading to a rapid rise in the evaporation rate and breakup of the liquid column.
2. The heater surface was a small rectangular plate located on the side of a pool. Consequently the liquid column was confined on three sides by walls rather than being surrounded by a vapor film. Thus, the liquid configuration would be relatively stable compared to the real case where a freestanding column of liquid would be subject to large-scale oscillations in addition to the surface perturbations observed here.
3. In this flat plate experiment, there is no vapor generation upstream of the leading edge, whereas during reflood there is violent boiling at the quench front thereby providing an initial source of vapor to the film and also perturbing the film. In contrast, for this experiment, the film is initially smooth and only develops ripples and large waves some distance downstream as the vapor flow rate increases. This contrasting behavior was recently noted by UCLA while performing steady state film boiling tests using a "hot patch" to freeze the quench front (see section V.2 below).

4. Due to the configuration of the vertical channel used in this experiment, it is not obvious what characteristic length should be used when converting the measured interfacial heat transfer coefficient into a Nusselt number for correlation purposes. For example:
    a. Hydraulic diameter: if the entire wetted perimeter is used to calculate this characteristic dimension, is value is 3.93 cm.
    b. Heated diameter: if only the heated perimeter is used, the resulting characteristic dimension has a value of 20.61 cm.
    c. Thickness: if the thickness of the liquid core is considered to correspond to the radius of the liquid core, then the characteristic dimension is 8.26 cm.

To address the above deficiencies caused by the non-prototypical geometry, this task order was modified to include a task on post-CHF heat transfer in a rod bundle geometry as discussed below.

V.2. UCLA Single-Rod Tests

The UCLA single-rod tests were not an experimental program unto themselves. Rather this was a subtask of the rod bundle experiment described in the next section. The purpose of these tests was to determine the requirements for effective operation of a "hot patch" integrated into a heater rod so that it could be used in the rod bundle tests.

The hot patch technique is to supply enough separate power to a short section just ahead of the test section to reach CHF, thereby preventing the rewetting front from advancing. This technique allows steady-state subcooled flow film boiling experiments to be run without running the entire test section at high power. It was first used in freon experiments by Groeneveld (1974). Later, to increase the power of the hot patch so that water could be used as the coolant, Groeneveld & Gardiner (1978) used a thick copper cylinder equipped with a number of cartridge heaters as depicted in Figure 12a for an indirectly heated hot patch applied to a tubular test section.

To allow operation at higher hot patch powers but avoid some of the problems other experimenters had experienced with contact losses between the copper blocks and the test section, Chen & Li (1984) developed a directly heated hot patch technique. As shown schematically in Figure 12b, the tubular test section included relatively short grooves where the wall thickness was reduced locally, so that a heat flux peak could be created due to the higher electric resistance. For the groove at the entrance of the test section, a separate power supply was provided so that the advancement of the quench front could be arrested at that location. A second groove at the top of the test section prevented the top-down progression of a quench front from the unheated region above the test section. In addition to avoiding contact problems between the hot patch and the test section, this directly heated method also controlled the location of the quench front more precisely due to its shorter length.

Figure 12: Schematic diagram of test sections equipped with (a) indirectly, and (b) directly heated hot patches.

Figure 13 (Chen 2011) illustrates the efficacy of the hot patch technique in providing steady-state subcooled film boiling conditions. Comparing Figure 13 (a) and (b), we see a similar effect of subcooling upon the vapor-liquid interface as that depicted above in Figure 8. The third image in Figure 13 shows the advancement of the quench front into the test section when the hot patch is turned off. As stated above, although such transient data could be used for model development, it is difficult to quantify the heat release at the quench front and hence the inlet conditions for the film boiling region.

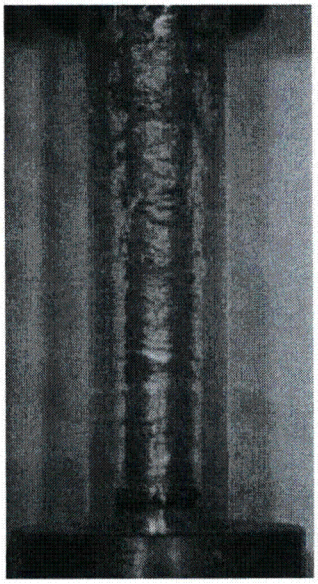

Figure 13: Inverted annular film boiling in an annulus with water flowing upwards: (a) and (b) Stable regime with the hot patch on, $T_{l,a} < T_{l,b}$, and (c) Reflood transient with the hot patch off.

Although the hot patch technique has been used very successfully for tubular test sections, the challenge for this task order was the design of a hot patch that could effectively stabilize the quench front at the test section inlet for a rod bundle. UCLA solved this problem with the rod design depicted in Figure 14 and Figure 15 below. The heat source for the film boiling region was a directly heated tube (either stainless steel or zircaloy) while the hot patch power was supplied by a cartridge heater embedded within the rod. In the film boiling region, the interior of the rod was filled by an aluminum silicate (lava) rod to add thermal inertia to help stabilize temperatures and to provide for positioning the wall thermocouples against the inner surface of the tube wall. At the location of the hot patch, the cartridge heater was enclosed in a cylinder of boron nitride both to electrically insulate the heater from the tube wall and to provide a high conductivity material to transfer the heat to the tube wall. Also, note the provision of two thermocouples at the location of the hot patch to provide temperature control for the cartridge heater power and to determine the axial position of the frozen quench front.

Figure 14: Cross-section of heater rod assembly: (a) with hot patch, and (b) without hot patch.

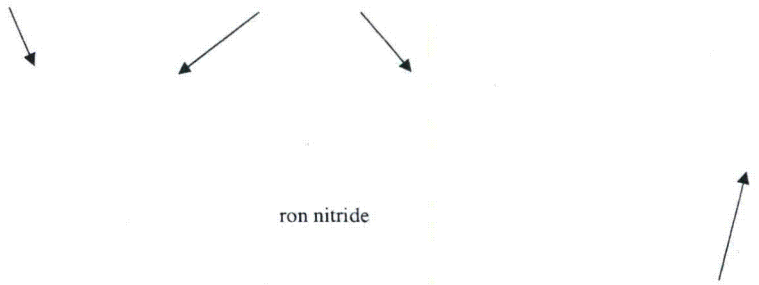

Figure 15: Cross-sectional view of hot patch showing location of cartridge heater.

To stabilize the quench front in a test section cooled by water requires a very high hot patch power. For example, a typical tubular test section (with an ID = 12 mm, and heated length of 80 cm) required the use of 8 cartridge heaters each with a power rating of 250 W to freeze the quench front for a test at atmospheric pressure, a mass flux of 500 (kg/m^2s), and an inlet subcooling of only 20 °C. The required hot patch temperature was over 500 °C and the hot patch power was about 30% of the entire power applied to the test section. These power requirements, together with the objective of keeping the length of the hot patch as short as possible to better locate the quench front, ruled out the use of water as the coolant for the proposed rod bundle film boiling tests.

For these reasons and others discussed in the next section, it was decided to use a simulant fluid, specifically Fluorinert FC-72 (also referred to as PF-5060) due to its low latent heat and low boiling point. As a result, the hot patch power was only a few percent of the test section power while the wall superheat required to stabilize the quench front was only about 150 °C. For example, typical values for the wall heat flux in the film boiling region were about 6-7 (W/cm^2) with an additional 2-4 (W/cm^2) applied at the hot patch that was only 2.54 cm in length. In contrast, for a water-cooled experiment at the same flow conditions, the film boiling heat flux would be about 20-30 (W/cm^2) with an additional 60-70 (W/cm^2) required for the hot patch.

Figure 16 gives a schematic of the single-rod test section while Figure 17 is a photograph of it fully instrumented and installed in the flow loop. The heater rod described above had an outside diameter of 1.11 cm and a heated length of 71 cm. The rod was inserted concentrically within a glass tube having an ID of 1.59 cm, creating an annular flow channel with a gap width of 2.4 mm. This geometry provides a hydraulic diameter, based on the heated perimeter, of 1.168 cm that is equal to that of the RBHT rod bundle used in the reflood experiments conducted for the NRC by Penn State.

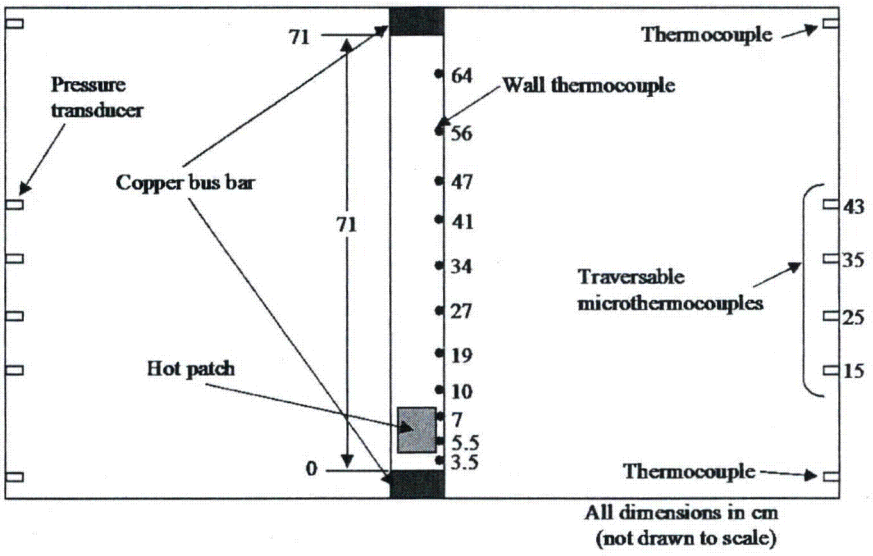

Figure 16: Schematic of the UCLA single-rod test section.

Despite the purpose of the single-rod tests being the shakedown of the heater rod and hot patch design, the test section was instrumented in a manner similar to that planned for the follow-up rod bundle tests. A total of 11 wall thermocouples were installed along the heated length together with 6 fluid thermocouples (for liquid-core subcooling) and 6 pressure taps (to measure differential pressure from which the void fraction can be inferred). The data from these single-rod tests would then form a useful baseline for the data from the rod bundle tests helping to quantify differences due to the geometry.

The traversing micro-thermocouples were intended to serve a dual purpose. First, to measure the bulk temperature of the liquid core so that the liquid-side interfacial heat transfer coefficient could be inferred using the procedure described in Section III and given by equation (17). Secondly, to attempt to measure the radial liquid temperature profiles as was done in the UCLA vertical plate film boiling tests described in Section V.1 above. These attempts were not very successful due primarily to the fact that while traversing, most of the micro-thermocouples made contact with the heater rod and were consequently destroyed. Hence, no liquid temperature profiles were reported.

Figure 17: Photograph of the UCLA single-rod test section.

A series of 20 subcooled film boiling experiments were successfully conducted in the single-rod test facility to confirm the operation of the hot patch design and determine its operating requirements for the planned rod bundle tests. The test matrix is given in Table 1 below. The hot patch performed well in all of these tests and the design was approved for use in the follow-on rod bundle tests. The results of these tests, with respect to wall heat transfer, were reported in Yi et al (2009). An example of the test results for wall heat transfer is given below in Figure 18.

Table 1: Experimental conditions for UCLA single-rod tests.

Run	G	V	Superheat	Inlet subcooling	Pressure	q - rod	q - cartridge
	($kg/m^2 s$)	(m/s)	(°C)	(°C)	(bar)	(W/cm^2)	(W/cm^2)
1	235	0.14	269	24.8	1.18	6.5	2.3
2	318	0.19	256	18.9	1.11	6.1	2.7
3	492	0.3	254	15.3	1.04	6.1	2.4
4	410	0.25	219	23.6	1.08	5.5	3.9
5	470	0.29	261	23.5	1.07	6.5	2.8
6	513	0.31	308	23.6	1.05	7.7	2.0
7	768	0.47	212	14	1.03	5.4	3.3
8	811	0.5	260	13.6	1.03	6.8	2.3
9	812	0.5	286	13.5	1.03	7.7	1.8
10	632	0.39	283	22	1.16	7.4	2.6
11	578	0.36	230	21	1.15	6.1	3.5
12	567	0.34	273	26.8	1.16	7.1	2.7
13	604	0.37	296	26.8	1.16	7.8	2.1
14	296	0.18	224	20.2	1.15	5.4	3.3
15	260	0.16	298	19.9	1.11	7.3	1.2
16	493	0.3	228	18.5	1.12	5.6	2.7
17	519	0.32	303	18.7	1.10	7.7	1.0
18	574	0.35	280	22	1.06	6.9	2.2
19	516	0.31	212	20.8	1.04	5.2	4.2
20	227	0.14	211	21.4	1.04	4.7	2.9

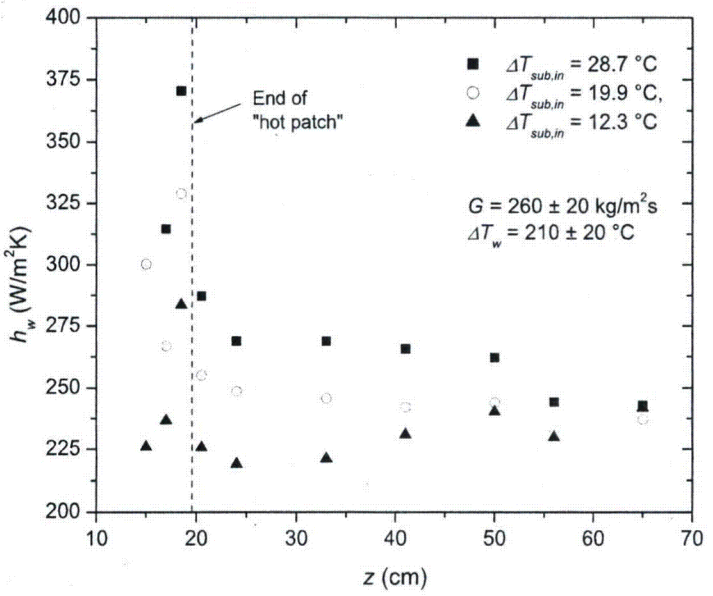

Figure 18: Effect of inlet subcooling on wall heat transfer coefficient.

Although these tests were successful for the most part in looking at the wall heat transfer, they were not particularly successful in quantifying the liquid-side interfacial

heat transfer. First, as noted above, the technique of measuring the radial liquid temperature profile did not work for these tests. Also, there was a problem with the bulk liquid temperature measurements recorded for two of the six fluid thermocouples as illustrated in Figure 19 where there appears to be an almost linear axial profile for the bulk liquid temperature from the inlet to the exit. However, the readings for the two thermocouples at 35 and 43 cm display a non-monotonic behavior that would be unphysical. The results depicted in this figure are typical of those for all 20 of the tests, consequently, it was concluded that these two thermocouples systematically read low temperatures. As the single-rod tests were only a proof-of-principle for the hot patch design, the reasons for these low readings were never uncovered nor corrected.

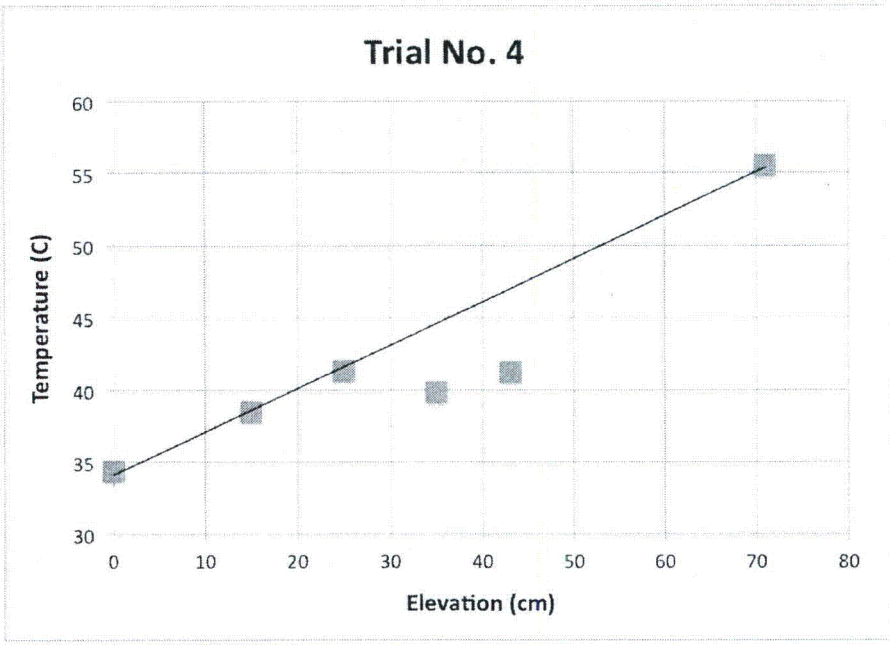

Figure 19: Axial profile of the bulk liquid temperature for Trial #4 of the UCLA single-rod tests.

In an undergoing model development effort, due to the aforementioned problems with the fluid thermocouples, it was necessary to disqualify data from these two points. Recalling that the hot patch is located between 5 and 7.5 cm, and that the exit thermocouple (located at 71 cm) may not be in IAFB, the only data span for the liquid temperature differential that may be considered valid for the evaluation of the liquid-side interfacial heat transfer is that between 15 and 25 cm.

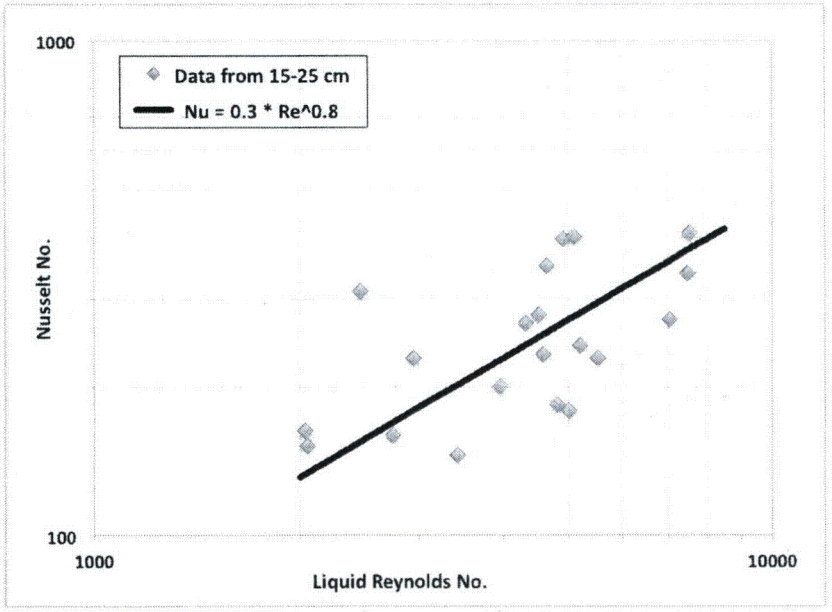

Figure 20: Values for the liquid-side interfacial heat transfer coefficient inferred from the data from the fluid thermocouples at 15 and 25 cm in the UCLA single-rod tests.

Figure 20 plots the Nusselt number for liquid-side interfacial heat transfer against the Reynolds number for the liquid core for all 20 of these tests using only the data from the fluid thermocouples at 15 and 25 cm. There is substantial scatter for these inferred values, which is not unusual for tests concerned with interfacial heat transfer. Some of this scatter is probably due to the effect of subcooling that was noted above for the UCLA vertical flat plate tests. The solid line plotted in this figure seems to indicate that the Nusselt number for liquid-side interfacial heat transfer has a dependence upon the liquid Reynolds number to approximately the 0.8 power corresponding to that expected for turbulent flow. This is in stark contrast to the results reported above for the vertical plate tests that indicated a dependence only to about the 0.2 power. Therefore, resolving the magnitude of the liquid-side interfacial heat transfer, its dependence upon liquid mass flux, and perhaps on subcooling, remains a critical data need for the improvement of the TRACE model for IAFB.

V.3. UCLA Rod Bundle Experiment

Upon the successful demonstration of the hot patch design in the single-rod experiments, the go-ahead was given for the rod bundle experiment described below. Unfortunately, the rod bundle film boiling experiment was not concluded successfully before the end of the Thermal Hydraulic Institute contract. Most of the problems encountered have to do with the home-built nature of the heater rods. In particular, the rod bundle facility experienced:

- In the initial attempt to establish film boiling conditions in the test section, one heater rod burned out. As a result, all testing was halted and the rod bundle was removed from the test loop and disassembled. Upon inspection of the damaged rod, it was found that the outer Zr-4 tube was intact and that only the cartridge

heater had burned out. However, the rod design[4] does not allow for the replacement of the cartridge heater and a new rod had to be fabricated.

- During the second attempt to run steady-state film boiling tests, film boiling conditions were successfully established on all 9 rods. However, after a few minutes of running two more of the cartridge heaters used in the bottom hot patch burned out despite being operated at only about 25% of their rated power of 250 W. This again necessitated replacement of the rods and, as no spares were available, new rods had to be fabricated.
- During preliminary testing of the reassembled rod bundle, it was found that almost all of the thermocouples in the bundle gave erratic readings once the DC power to the heater rod sheaths was turned on. The thermocouples used to measure wall temperature in the heater rods lie in a groove machined in the lava rock insert and are held in place using high temperature epoxy. Some of these thermocouples were apparently not adequately electrically insulated from the rod sheath, which is a thin-walled tube with DC Joule direct heating. Consequently, these "bad" thermocouples picked up some voltage and affected the readings of the other thermocouples. Identifying which thermocouples were bad and disassembling and repairing the heater rods caused another delay.

Despite the above problems, based on the successful operation of the single-rod tests, UCLA expressed confidence that the approach would work for a rod bundle. However, it was suggested that a better power control system for the hot patches be used. Specifically, an automated power control system using the readings from the thermocouples at the hot patch location should be used rather than the manual adjustments used for the current test rig.

As briefly discussed above, a simulant working fluid with low latent heat and boiling temperature was selected for these experiments. The particular working fluid chosen was Fluorinert FC-72, which was the only fluid with the desired heat transfer properties that also met the environmental restrictions in California. The reasons for choosing the use of a simulant working fluid for the rod bundle tests were partially discussed above; a more complete listing is given below:

- The wall temperatures in the film boiling region for FC-72 are on the order of 250-350 °C versus 700-1000 °C for water.
  - This allows the use of a small rod bundle (such as a 4x4) without significant distortions due to radiation heat transfer.
  - Heat losses from the bundle are small due to the reduced operating temperatures, again very important in allowing the use of a small rod bundle.
  - Lower operating temperatures allow for the use of transparent test section walls enabling visual observation and possibly optical instrumentation.
  - Problems caused by thermal expansion of the rods and sealing of the rod penetrations are minimized.
- The hot patch power required to stabilize the quench front is a factor of 10-20 times smaller than that for water.

[4] The copper bus bars are shrink fit onto the ends of the Zr-4 heater tubes and so cannot be opened up for replacement of the cartridge heater.

- This greatly simplifies the design of the hot patch allowing for its use in a rod bundle where the heat source must be embedded within the rods.
- It allowed a relatively short hot patch (2.54 cm) to be used providing for better localization of the quench front. Even shorter hot patches could be realized if smaller cartridge heaters were available or a different rod design used[5].
- For FC-72, the hot patch power required was only a few percent of that for the film boiling region whereas for water it can be as high as 40%. This greatly reduces the uncertainty associated with the fluid state at the beginning of the film boiling region and allows testing with larger subcoolings in the IAFB region.
- The reduced hot patch power requirements provide a greater flexibility in extending the mass flux and inlet subcooling range.

- The different fluid properties of a simulant working fluid allow for high-pressure conditions to be simulated in a bundle operating at low pressure. Thus the data would serve to complement that of the RBHT facility (max operating pressure of about 4 bar) and better simulate the blowdown rewet conditions of the LOFT experiments.

For the above reasons, a simulant working fluid was chosen for the UCLA rod bundle film boiling experiment and is recommended for the proposed future experimental program. The remainder of this section describes the UCLA rod bundle.

The heater rod design for each of the nine rods in the bundle was similar to that of the single-rod heater used in the hot patch tests. A schematic is given in Figure 21 and the main characteristics were:

(a) Total length = 74.6 cm.

(b) The material of the outer DC Joule heated tube is Zircalloy-4.

(c) The wall thickness of the Zr-4 tubes is 0.2 mm.

(d) Two "hot patches" were incorporated into the heater. One close to the bottom and the other at the top to prevent top down quenching.

(e) Number of wall thermocouples in each rod is 11. The axial location of the thermocouples is given in Table 2.

[5] In the Rod Bundle Heat Transfer (RBHT) test facility operated for the NRC by Penn State, the heater rods were manufactured by Stearn Laboratories and have proved to be very robust. These rods are indirectly heated employing a thin-walled tube within the rod as the resistance element; an axially varying heat flux profile was provided by varying the thickness of this tube. As a heat flux spike of only about 50% is needed to freeze the quench front for a fluid such as FC-72, a notched type of hot patch could be employed. However, the probable need to provide power control for the hot patch would complicate this design.

Table 2: Axial location of wall thermocouples.

Thermocouple	Location (cm)
1	3.8
2	5.7
3	7.6
4	12.7
5	20.3
6	27.9
7	35.6
8	43.2
9	50.8
10	62.2
11	71.1

s in cm.
Not drawn to scale

Figure 21: Details of heater rod design.

The nine rods were arranged in a 3x3 square array as shown below in Figure 22. The 3x3 array has a pitch of 1.5 cm and is installed in a square housing with an inner dimension of 4.5 cm. The resulting hydraulic diameter, based on heated perimeter, is therefore 1.471 cm for all three subchannel types (normal, edge, and corner) present in the bundle. Constraining the ratio of the flow area to heated perimeter to be the same for all subchannels results in the bundle average void fraction and the void fraction in the individual channels being approximately the same for inverted annular flow.

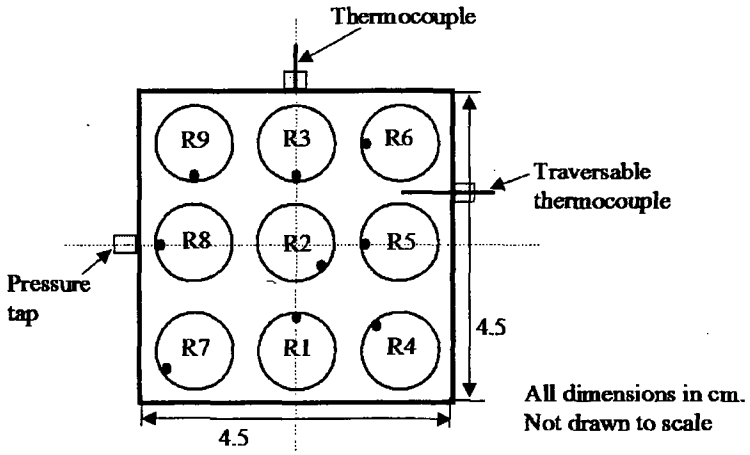

Figure 22: Cross-section of 9-rod bundle.

The schematic of the complete test section is shown in Figure 23. The test section is made from aluminum (0.64 cm thick) and is provided with glass windows (0.64 cm thick) on all four sides for visual observation. The glass windows are present along the entire length of the test section. Pressure and liquid temperatures were measured at six axial locations along the test section (inlet, z = 14.0 cm, z = 30.5 cm, z = 47.0 cm, z = 63.5 cm, and outlet). In addition, traversable micro-thermocouples, to measure the fluid temperature at the centroids of interior subchannels, are also provided at four axial locations as shown in Figure 23: (z = 14.0 cm, z = 30.5 cm, z = 47.0 cm, z = 63.5 cm). One key feature of the traversable micro-thermocouples is that they can be completely withdrawn from the test section. This allows for liquid temperatures to be measured at a lower elevation and then the thermocouple withdrawn so that temperatures further downstream can be measured without flow perturbations.

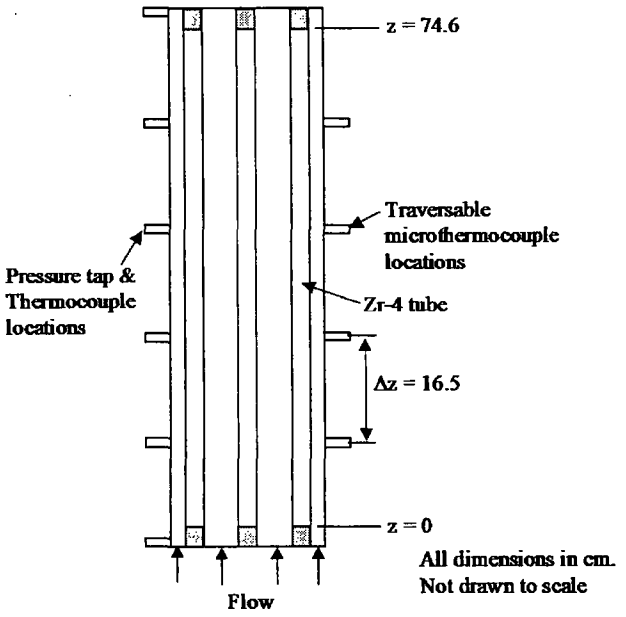

Figure 23: Schematic of the 9-rod bundle test section.

As stated above, despite the failure of this experimental program to be completed before the end of the previous Thermal Hydraulic Institute contract, significant enough progress was made to warrant a follow-up experimental program. To improve the chances of success, any follow-up program should:

- Use professionally manufactured heater rods (if possible) to avoid the difficulties that were encountered in the UCLA program using "home-built" rods.
- Use a suitably designed automatic power control system for the hot patch power based on feedback from the hot patch thermocouples rather than manual adjustments.
- Make adequate provisions for spare heater rods so that long delays do not ensue if a rod fails and needs replacement.

This completes the description of the UCLA rod bundle post-CHF heat transfer experiment.

VI. REFERENCES

Arai, T. Furuya, M., Kanai, T. and Shirakawa, K., (2012), "Development of a Subchannel Void Sensor and Two-phase Flow Measurement in a 10x10 Rod Bundle," *Int. J. Multiphase Flow*, **47**, 183-192.

Chen Y. & Li, J. (1984), "Subcooled Flow Film Boiling of Water at Atmospheric Pressure," in *Two-phase Flow and Heat Transfer*, X. J. Chen and T. N. Veziroglu, 141–

150, Hemisphere Pub. Co., ISBN 0-89116-432-4.

Chen, Y. (2011), "Heat Transfer in Film Boiling of Flowing Water," in *Heat Transfer - Theoretical Analysis, Experimental Investigations and Industrial Systems*, Aziz Belmiloudi (Ed.), ISBN: 978-953-307-226-5.

de Cachard, F., (1996), Development, Implementation and Assessment of Specific, Closure Laws for Inverted-Annular Film Boiling in a Two-Fluid Model, NUREG/IA-0133.

El Nakla, M. Groeneveld, D.C., and Cheng, S.C., (2011), "Experimental Study of Inverted Annular Film Boiling in a Vertical Tube Cooled by R-134a," *Int. J. Multiphase Flow*, **37**, 67-75.

Fung, K. K., (1981), Subcooled and Low Quality Film Boiling of Water in Vertical Flow at Atmospheric Pressure, Ph. D. Thesis, University of Ottawa, Canada.

Groeneveld, D. C. (1974), "Effect of a Heat Flux Spike on the Downstream Dryout Behavior," *J. of Heat Transfer*, **96c**, 121-125.

Groeneveld, D.C, and Gardiner, S.R.M. (1978), "A Method of Obtaining Flow Film Boiling Data For Subcooled Water," *Int. J. Heat Mass Transfer*, **21**, 664-665.

Hammouda, N., Groeneveld, D.C., and Cheng, S.C., (1996), "An Experimental Study of Subcooled Film Boiling of Refrigerants in Vertical Up-flow," *Int. J. Heat Mass Transfer*, **39**, 3799-3812.

Manera, A., Ozar, B. Paranjape, S., Ishii, M., and Prasser, H.-M., (2009), "Comparisons Between Wire-Mesh Sensors and Conductive Needle-Probes for Measurements of Two-Phase Flow Parameters," *Nuclear Eng. and Design*, **239**, 1718-1724.

Meduri, P.K., (2007), "Wall Heat Flux Partitioning During Subcooled Flow Film Boiling of Water on a Vertical Surface," Ph.D. thesis, Dept. of Mechanical Engineering, University of California, Los Angeles, CA.

Meduri, P.K., Warrier, G.R., and Dhir, V.K. (2006), "Flow Film Boiling on a Vertical Flat Plate at Different Subcoolings and Flow Velocities," 13th International Heat Transfer Conference, Sydney, Australia.

Meduri, P.K., Warrier, G.R., and Dhir, V.K. (2009), "Wall Heat Flux Partitioning During Subcooled Flow Film Boiling of Water on a Vertical Surface," *Int. J. Heat Mass Transfer*, **52**, 3534-3546.

Yi, S., Warrier, G.P., and Dhir, V.K., (2009) "Heat Transfer and Hydrodynamics of Subcooled Inverted Annular Flow Film Boiling on a Single Rod Heater," Proceedings of the ASME 2009 International Mechanical Engineering Congress, Lake Buena Vista, FL, Paper no. IMECE2009-12694, 1709-1718.

Attachment #2: Hot Patch Design Study

Objective

The objective of this study is to determine the feasibility of performing low-quality steady-state film boiling experiments for a directly heated tube using water as the coolant. In addition, this study aims to provide guidance as to a possible design for the "hot patch" that will be used to stabilize the quench front for steady-state film boiling tests at high pressure and flow conditions.

Background

The constitutive models for two post-CHF flow regimes have been identified as high priority items for improvement involving near-term experimental programs: inverted annular film boiling (IAFB) and inverted slug film boiling (ISFB). For both of these regimes, there is a critical need for accurate void fraction measurements over a wide range of flow conditions. To facilitate both the needed void fraction measurements and the subsequent model development activity, it would be preferable to conduct steady-state experiments. To do so requires a means of "freezing" the quench front and that is the subject of this study.

The operating principle of the hot patch technique is to supply enough separate power to a short section just ahead of the test section to reach CHF, thereby preventing the rewetting front from advancing. This technique allows steady-state subcooled flow film boiling experiments to be run without running the entire test section at high power and was first used in Freon experiments by Groeneveld (1974). Later, to increase the power of the hot patch so that water could be used as the coolant, Groeneveld & Gardiner (1978) used a thick copper cylinder equipped with a number of cartridge heaters as depicted in Figure 1a for an indirectly heated hot patch applied to a tubular test section.

To allow operation at higher hot patch powers but avoid some of the problems other experimenters had experienced with contact losses due to cracking of the braze between the copper blocks and the test section, Chen & Li (1984) developed a directly heated hot patch technique for experiments conducted by the Chinese Institute for Atomic Energy (CIAE). As shown schematically in Figure 1b, the tubular test section included relatively short grooves where the wall thickness was reduced locally so that a heat flux peak could be created due to the higher electric resistance. For the groove at the entrance of the test section, a separate power supply was provided so that the advancement of the quench front could be arrested at that location. A second groove at the top of the test section prevented the top-down progression of a quench front from the unheated region above the test section[1]. In addition to avoiding contact problems between the hot patch and the test section, this directly heated method also controlled the location of the quench front more precisely due to its shorter length and resulted in fewer distortions of the film boiling region just downstream of the quench front.

---

[1] In one paper (Chen et al, 1988), it was found necessary to also independently power the top hot patch to prevent top-down quenching at high flow conditions.

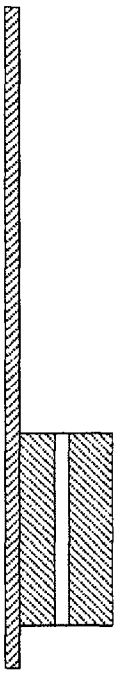

Figure 1: Schematic diagram of test sections equipped with (a) indirectly, and (b) directly heated hot patches.

Figure 2 (Chen 2011) illustrates the efficacy of the hot patch technique in providing steady-state subcooled film boiling conditions for inlet conditions with both high subcooling (Figure 2a) and low subcooling (Figure 2b). The third image in Figure 2 shows the advancement of the quench front into the test section when the hot patch is turned off. Although such transient data could be used for model development, it is difficult to quantify the heat release at the quench front and hence the inlet conditions for the film boiling region.

Through a series of experimental programs, this directly heated hot patch technique was steadily improved until Chen et al (1989) were able to conduct steady-state film boiling experiments at pressures up to 60 bar. Specifically, the range of test conditions covered was:

Pressure:	4.1 – 60 (bar)
Mass Flux:	48 – 1462 (kg/m^2s)
Inlet Quality[2]:	-0.05 – 0.24
Heat Flux:	28 – 260 (kW/m^2)

[2] Refers to the equilibrium quality at the dryout point, assumed to be located at the top of the bottom "hot notch".

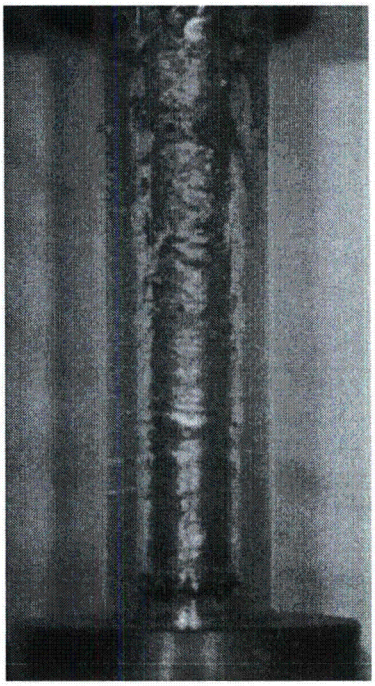

Figure 2: Inverted annular film boiling in an annulus with water flowing upwards: (a) and (b) Stable regime with the hot patch on, $T_{l,a} < T_{l,b}$, and (c) Reflood transient with the hot patch off.

For these high-pressure tests, the test section was made of Inconel-600 tubing with a 12 mm ID and 15 mm OD as shown in Figure 3 below. The film boiling length (section BC) was 2.2 m, and the length of the bottom hot patch (section AB) varied from 25 mm to 50 mm in order to study the effect of the upstream heating condition. Both sections were direct heated using AC power supplies with the terminals located at points A, B, and C as shown in the figure. These power terminals were made from stainless steel sheets that were argon welded onto the tube and had a thickness of 1.5 mm.

The small notches, machined just upstream of the power terminals at points B and C, are 0.7 mm in depth, 1 to 2 mm in length, and cause higher electrical resistances creating heat flux peaks to stabilize the quench front. After establishment of the film boiling regime, the quench front was maintained just 1 to 2 mm upstream of point B and the flow was very stable. In this experimental campaign, Chen et al (1989) conducted a total of 151 successful test runs and noted that "no trouble was encountered at the highest pressure." This successful operation was observed despite the reduced tube wall thickness at the notch being only 0.8 mm thick.

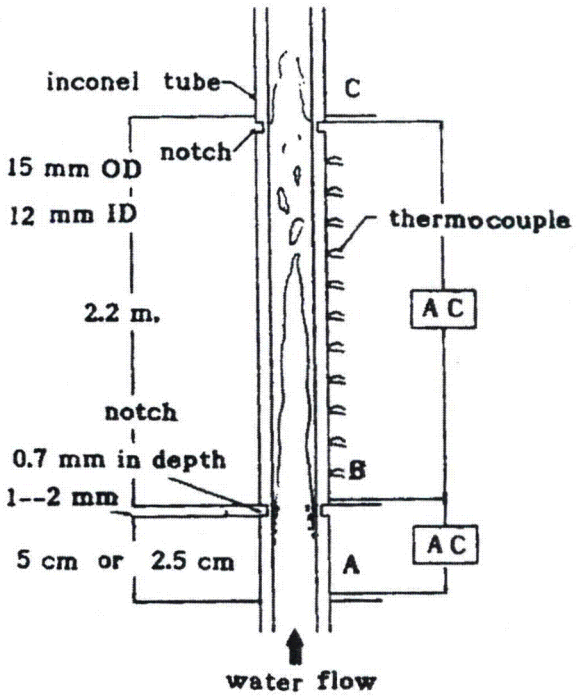

Figure 3: Schematic of test section with directly heated hot patch (Chen et al, 1989).

Steady-state low-quality film boiling experiments were also conducted at Winfrith in the UK. For their first three series of tests an indirectly heated hot patch of the type pioneered by Groeneveld was used. This technique appeared to work reasonably well at low-pressure conditions, however, as detailed by Swinnerton et al (1988) the braze connecting the copper hot patch to the test section developed circumferential cracks at high-pressure conditions. The contact resistance attributed to these cracks resulted in ever-increasing hot patch power requirements in order to stabilize the quench front thereby greatly limited the effective operating range and preventing reproducibility of their data.

Consequently, for the last two series of film boiling tests, Winfrith switched to a directly heated "hot notch" type of hot patch as developed by Chen et al for the CIAE and described above. In their Series 4 tests (Savage et al, 1992) the film boiling length was 0.92 m, while the addition of sapphire viewing ports at 0.79 m above the hot patch reduced the effective film boiling length to 0.71 m for the Series 5 tests (Savage et al, 1993). For both series the test section was comprised of Inconel-600 tubing with a 9.42 mm ID and a 12.68 mm OD. Three stainless steel discs were welded onto the tube at the positions shown in Figure 4. Independent AC power supplies were connected between the lower and middle disc, and between the upper and middle disc, which enabled the heat flux to the two regions of the tube to be separately controlled. Both the middle and upper discs were 1.6 mm thick, while the lower disc was 3.2 mm thick. The distance between the top of the lower disc and the bottom of the middle disc was 25 mm.

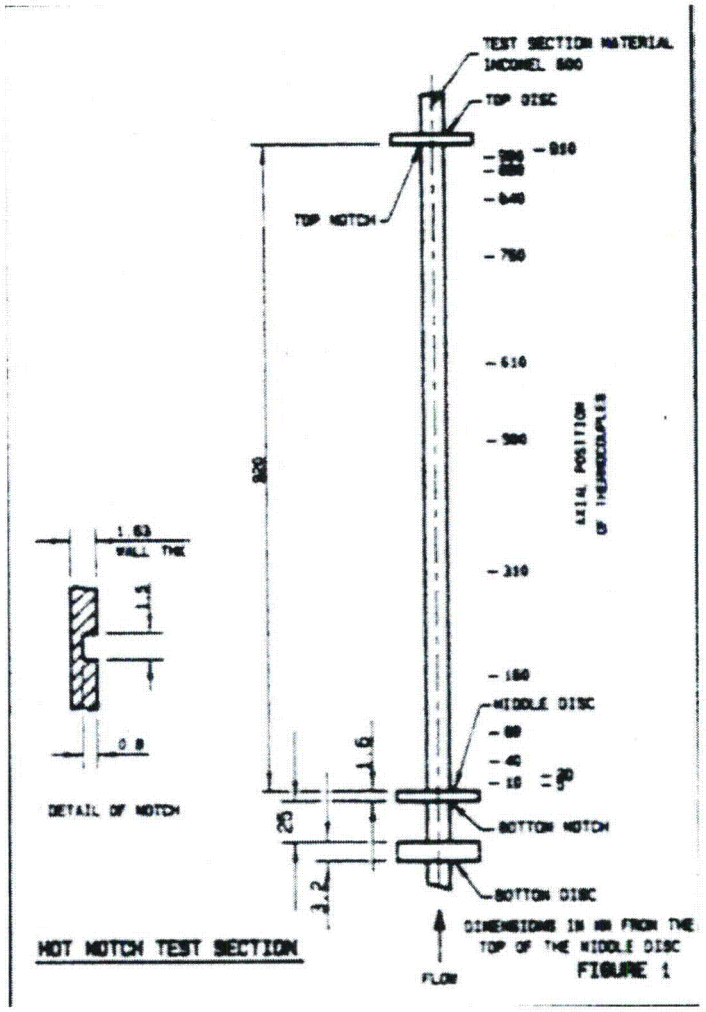

Figure 4: Schematic of the Winfrith Series 4 Test Section (Savage et al, 1992).

Small circumferential notches were machined in the outer wall of the tube immediately below the middle and upper discs. These notches provided the high resistance, high heat flux regions needed to stabilize the quench front and were denoted as "hot notches." These notches were similar in design to those used in the CIAE tests, having a depth of 0.8 mm and a length of 1.5 mm. The surface temperature of the notches was measured using bare wire precision welded thermocouples and was used to control the lower hot patch power.

Using this directly heated hot notch design, Winfrith was able to successfully conduct steady-state film boiling tests for:

Pressure:	5 – 70 (bar)
Mass Flux:	100 – 1000 (kg/m^2s)
Inlet Subcooling:	18 – 50 (°C)

Savage et al (1993) commented that "the hot notch test section operated well over a range of conditions, but has a short working life of less than 40 hours." Unfortunately, no details were given as to what limited the working life of the test section and so it is not known if the limiting factor was related to the reduced tube wall thickness of only 0.83 mm or to the sapphire windows. Nevertheless, while both CIAE and Winfrith were able to safely conduct high-pressure film boiling tests, at 60 and 70 bar respectively, the development of a more robust test section design is one of the goals of this design study.

Test Section Design

For this study, the directly heated hot patch technique was adopted. The reasons for this deign choice were:

- The problems that Winfrith experienced with cracking of the braze between the copper hot patch and the Inconel test section when using the indirectly heated technique (Swinnerton et al, 1988).
- Better localization of the quench front with the notch-type hot patch that has a length of a few millimeters as opposed to the large copper block type that has a length of 25 to 100 mm.
- Less distortion at the entry to the film boiling region and allowance of measurements closer to the dryout point.

In both the CIAE and Winfrith experiments Inconel-600 tubing was used for the test section due both to its mechanical strength at high temperature and its relatively temperature independent electrical resistivity. For both of these reasons, and its ready commercial availability in a number of standard sizes, Inconel-600 was selected as the test section material here as well.

A number of other design criteria need to be considered as well. Specifically:

- The test section inside diameter should be in the range of the hydraulic diameter for modern BWR and PWR fuel assemblies,
- The tubing OD and wall thickness should correspond to that of commercially available Inconel-600 tubing,
- The wall thickness should be maximized to provide strength for high-temperature high-pressure conditions,
- The notch length should be as short as possible to better localize the quench front and minimize the distortion at the entry to the film boiling region,
- The notch depth should be as deep as possible to provide the necessary heat flux spike to stabilize the quench front but should not compromise the mechanical strength of the test section,
- The notch temperature should be as low as possible,
- The operating range for the hot patch power should be as large as possible to facilitate power control, and
- The pre-heater section, that is the separately powered region that contains the hot notch (see section AB of Figure 3), should be as short as possible so that the subcooling at the quench front is not too different from that of the inlet.

Through a consideration of these criteria and by performing a number of sensitivity studies, a workable directly heated hot patch design was obtained that should also be

more robust than that used in the CIAE and Winfrith experiments. This design will be described here and used as the base case for the sensitivity studies presented below.

A number of candidate off-the-shelf Inconel-600 tube sizes were considered based on a tubing selection guide from the Eagle Stainless Tube & Fabrication of Franklin, MA. The selected tube OD was 0.75" (19.05 mm) and the wall thickness was 0.12" (3.048 mm). This gives an inside diameter of 12.95 mm that satisfies the criterion of being in the range of hydraulic diameter for modern fuel assemblies as shown in the table below.

Reactor Type	Vendor	Assembly Type	Pitch (mm)	Rod OD (mm)	D_h (mm)
BWR	GE	8x8 Barrier	16.26	12.27	15.17
BWR	GE	8x8 GE-4a	16.26	12.52	14.37
BWR	Areva	9x9 JP 3-5	14.52	10.76	14.19
BWR	Areva	9x9 1X, 9X	14.45	10.95	13.33
PWR	Westinghouse	17x17 Vantage 5	12.6	9.14	12.98
PWR	RBHT	17x17	12.6	9.50	11.78

The wall thickness of the selected tubing is 3.048 mm that is nearly double that used in the CIAE (1.5 mm) and Winfrith (1.63 mm) experiments. The selection of a thicker walled tube was made to increase the robustness of the test section, especially for operation at high-pressure conditions. However, the thicker tube wall allows for more axial conduction at the quench front where the axial temperature profile is the steepest. To counteract the effect of this increase in axial conduction required changes to the notch geometry as described below.

First, let's introduce two design parameters that will affect the operability and robustness of the test section: 1) the ratio of the tube cross-sectional area to that of the notch, and 2) the hoop stress geometry factor. To stabilize the quench front, a local spike in the linear heat generation rate is introduced by machining a notch in the tube wall thereby decreasing the wall thickness and increasing the electrical resistivity and hence the heat generation rate. It is important to realize that this applied linear heat rate does not exceed the CHF value, were it to do so the test section would experience "burn out", perhaps literally. Rather this local heat generation spike needs to be just large enough to counteract the axial conduction from the notch to the wetted region below it.

For a directly heated tube, the linear heat generation rate is given by

$$q' = I^2 \cdot \frac{\rho}{A}$$

where

I : current (A)

ρ : electrical resistivity (Ω·m)

A : cross-sectional area (m^2)

The electrical resistivity is a property of the material and is temperature dependent. However, Inconel-600 was selected in part due to its relatively low temperature dependence and so in the ensuing discussion the resistivity will be treated as a constant. Also, as the current is constant for the hot patch region, that includes both the notch and a pre-heater section (see section AB of Figure 3), the ratio of the linear heat generation rate for the notch relative to that of the pre-heater is simply

$$\frac{q'_N}{q'_{PH}} = \frac{A}{A_N} = \frac{\left(D_O^2 - D_I^2\right)}{\left(\left(D_O - 2\cdot\delta_N\right)^2 - D_I^2\right)}$$

where

A_N : cross-sectional area for the notch region

D_O : tube outside diameter

D_I : tube inside diameter

δ_N : notch depth

For the hot patch geometries used by CIAE and Winfrith, this parameter has the values: 1.98 and 2.12 respectively. So, it seems like a successful design might need to have a value of about 2 for this area ratio. With the tubing geometry selected above (i.e., OD = 19.05 & ID = 12.95 mm), this would imply that a notch depth of about 1.4 mm would be needed.

The other design parameter concerns the hoop stress than would occur at the notched part of the tube. Assuming that the thin-walled tube assumption can be used, the hoop stress would be given by

$$\sigma \approx \Delta P \cdot \left(\frac{D_I}{2\delta}\right)$$

where δ is the tube wall thickness at the notch. Thus, to compare the ratio of the hoop stress at the same pressure conditions, one can compare the geometry factor given by the tube ID divided by twice the wall thickness. For the test sections used by CIAE and Winfrith, this hoop stress geometry parameter has the values: 7.5 and 5.67 respectively. So, to produce a more robust design, this geometry factor should have a value less than about 5. As discussed below, a notch depth of 1.5 mm was selected as the base case for this design study resulting in a hoop stress geometry factor of 4.18 and so satisfies this criterion. In addition, the much greater wall thickness at the notch, 1.55 mm for our base design versus 0.8 and 0.83 mm for the CIAE and Winfrith designs respectively, will provide more resistance to other mechanical stresses that may arise during fabrication, installation and operation.

Along with the above two design parameters, both the hot patch operating range and notch maximum temperature were used as criteria to select the notch length and depth. The hot patch operating range was defined as the difference between the minimum and maximum values of the hot patch power for which the quench front can be stabilized. At hot patch powers lower than the operating range, the test section will quench no matter that the applied heat flux is greater than the minimum film boiling point. Conversely, for hot patch powers higher than the operating range, the tube will dryout as the quench front recedes into the pre-heater section. The maximum notch temperature is simply that, the maximum value for the material temperature in the notch region and is important due to its effect on the mechanical strength of the region where the highest stresses will occur.

From the sensitivity studies described below, it was determined that the most significant factor affecting the hot patch operating range is the notch length. Indeed, for our base design conditions, the operating range increased from a value of only 14 (W) for a notch length of 2 mm to a value of 172 (W) for a notch length of 4 mm. Likewise, the notch power necessary to stabilize the quench front decreased from 1221 (W) to 860 (W) as the notch length increased from 2 to 4 mm. However, as the notch length increased more of the notch region was exposed to film boiling and so a small increase in its maximum temperature was observed. This together with the desire to keep the notch as short as possible to better localize the quench front led to the selection of 3 mm for the notch length corresponding to an operating range of 115 (W).

The notch depth exhibited the same trends on operating range, hot patch power and maximum notch temperature, as did the notch length. Specifically, the operating range increased from a value of 67 (W) for a notch depth of 1.4 mm to a value of 153 (W) for a depth of 1.6 mm. Also, though the hot patch power requirements decrease with notch depth, the resulting increases in the notch heat generation rate result in somewhat higher temperatures. Most importantly, to keep the hoop stress geometry factor as low as possible yet maximize the operating range, an intermediate value of 1.5 mm was selected for the notch depth.

The last design parameter to be determined is the length of the hot patch region itself, that is, the distance between the top of the bottom electrode and bottom of the middle electrode. For both the CIAE and Winfrith test sections this length had a minimum value of 25 mm. It is supposed that this value may be constrained by either the necessary mechanical connections for the power cables to the electrodes, or by fabrication limitations (e.g., clearance space needed to weld the electrodes to the tubing). Regardless of the controlling factor, a spacing of 25 mm should be achievable, as it has already been done. To maintain the subcooling at the inlet to the film boiling region as close to the inlet subcooling as possible, the length of this pre-heater section should be minimized. Consequently, a value of 25 mm has been selected for this length. This completes the description of the geometry selected for this design study; the following section describes the methodology used to calculate the hot patch performance.

Methodology

A thermal analysis was performed to determine the hot patch power and temperature requirements necessary to stabilize the quench front using the COMSOL Multiphysics finite element analysis code. No attempt was made to solve the two-phase flow equations; rather a steady-state equilibrium quality calculation was combined with the

wall temperature to specify an appropriate boiling curve as described below. In addition, a PID controller (Proportional-Integral-Derivative) was used to determine the hot patch power necessary to keep the notch temperature at a specified set point.

Boiling Curve

A complete boiling curve from single-phase liquid forced convection through film boiling was specified as a function of:

- Pressure
- Mass flux
- Wall superheat
- Local equilibrium quality

In doing so, an effort has been made to keep the wall heat transfer models as consistent as possible with those of the TRACE code. The notable exception to this is the film boiling heat transfer coefficient that would require a full two-fluid flow solution to implement the TRACE post-CHF constitutive model package.

Liquid single-phase forced convection is calculated using the Gnielinski (1976) correlation as given by

$$Nu_{FC} = \frac{(f/2)(\mathrm{Re}-1000)\cdot \mathrm{Pr}}{1+12.7\cdot(f/2)^{\frac{1}{2}}\left(\mathrm{Pr}^{\frac{2}{3}}-1\right)}$$

where the friction factor is evaluated using the smooth tube formula of Filonenko (1954),

$$f = \left[1.58\cdot \ln(\mathrm{Re}) - 3.28\right]^{-2}$$

and the local value of the liquid subcooling is determined from the equilibrium quality.

For nucleate boiling, the pool boiling correlation of Gorenflo (1993) was used. The pool boiling model of Gorenflo uses a reference point formulation and is given by

$$h_{PB} = h_0 \cdot F_P \cdot (q''/q''_0)^n \cdot (R_P/R_{P0})^{0.133}$$

where, for water,

$$h_0 = 5600 \quad (\mathrm{W/m^2-C})$$

$$q''_0 = 20{,}000 \quad (\mathrm{W/m^2})$$

$$F_P = 1.73\cdot P_r^{0.27} + \left(6.1+\frac{0.68}{1-P_r}\right)\cdot P_r^2$$

$$n = 0.9 - 0.3\cdot P_r^{0.15}$$

with P_r being the reduced pressure,

$$P_r = \frac{P}{P_{crit}}$$

and the surface roughness having the reference value

$$R_{P0} = 0.4 \quad (\mu\mathrm{m})$$

For boiling surfaces that have not been characterized, it is recommended that the roughness be taken to be 0.4 μm, so that the surface roughness term is unity and this is the approach used in TRACE and in this design study.

For the pre-CHF regime, the wall heat transfer coefficient is then taken to be the maximum of the values for forced convection and nucleate boiling as

$$h = \max\left[h_{FC},\ h_{PB}\cdot\left(\Delta T_{sat}/\Delta T_{liq}\right)\right]$$

In the above formula, it was necessary to convert the pool boiling heat transfer coefficient from a wall superheat reference, namely

$$\Delta T_{sat} = T_{wall} - T_{sat}$$

to one relative to the wall-to-liquid temperature difference

$$\Delta T_{liq} = T_{wall} - T_{liq}$$

The wall-to-liquid temperature difference will be used as the driving potential for all of the wall heat transfer coefficients in this model. This pre-CHF heat transfer coefficient will be used for all points where the wall temperature is less than the CHF point.

The point where the maximum heat flux occurs will be denoted as the CHF point, $\left(q''_{CHF}, T_{CHF}\right)$, and is characterized by both the critical heat flux and the wall temperature at which it occurs. This is the point where the heat transfer regime transitions from that where the liquid phase wets the wall (i.e., nucleate boiling), to the post-CHF regimes where liquid-wall contact is either transient (transition boiling) or non-existent (film boiling).

In TRACE, the role of the CHF model is two-fold:

1) Determine the transition point for the heat transfer regime, and
2) Serve as the anchor point for the transition boiling wall heat flux.

To accomplish this dual objective, the 1995 AECL-IPPE CHF look-up table (Groeneveld et al, 1996) was selected for TRACE and is used in this model. The AECL-IPPE CHF table is based upon an extensive database of CHF values obtained in tubes for a vertical upward flow of a steam–water mixture. While the database covers a wide range of flow conditions, the look-up table was designed to provide CHF values for tubes at discrete values of pressure, mass flux, and dryout quality. Three-dimensional linear interpolation is used to determine the CHF for conditions between tabulated values.

The wall temperature, T_{CHF}, at which CHF occurs is found by solving the equation

$$q''_{PB}\left(\Delta T_{CHF}\right) = q''_{CHF}\left(P, G, x_{eq}\right)$$

using the pool boiling model of Gorenflo. The other anchor point for the boiling curve is the minimum film boiling point that corresponds to the minimum heat flux condition and defines the switch from the transition boiling to the film boiling regime. The Groeneveld-Stewart model (Stewart & Groeneveld, 1981) for the minimum film boiling temperature, T_{min}, is used in TRACE and in this model.

The Groeneveld-Stewart correlation for saturated water (or positive quality conditions) is given by

$$T_{min,sat} = 557.85 + 44.1 \cdot P - 3.72 \cdot P^2$$

for pressures less than 9 MPa where $T_{min,sat}$ is in °K and P is in MPa. In their database, both the effects of mass flux and quality (for positive values) were deemed negligible. A significant effect of subcooling was observed and was correlated by

$$T_{min} = T_{min,sat} - \frac{x_{eq} \cdot 10^4}{(2.82 + 1.22 \cdot P)}$$

where x_{eq} is the subcooled quality. The resulting values for T_{min} are shown below in Figure 5 as a function of pressure and subcooling.

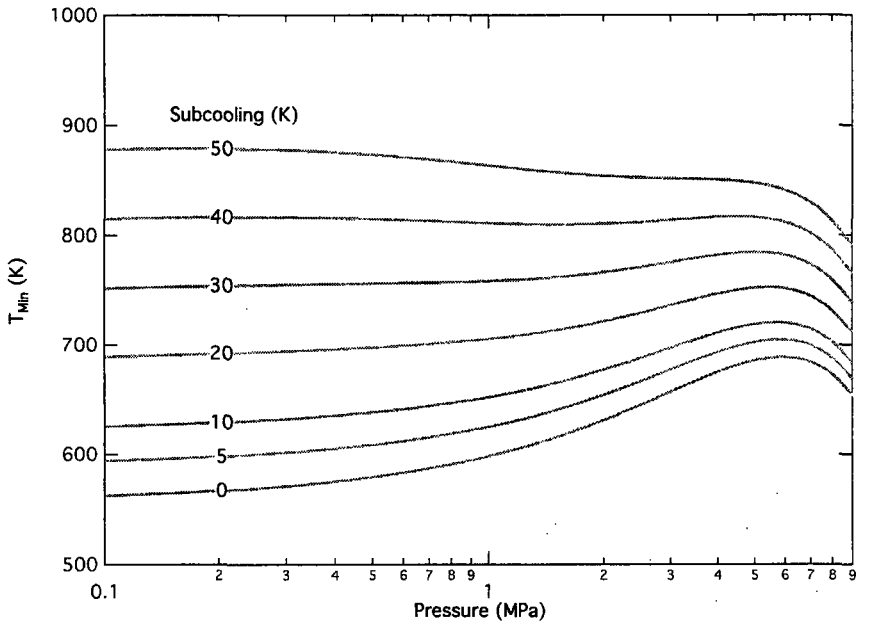

Figure 5: Values for the minimum film boiling temperature of Groeneveld & Stewart as a function of pressure and subcooling.

To complete the specification of the minimum film boiling (MFB) point, the heat flux is calculated from

$$q''_{min} = h_{FB}\left(P, G, x_{eq}, \Delta T_{min}\right) \cdot \left(T_{min} - T_{sat}\right)$$

where the film boiling heat transfer coefficient is a function of pressure, mass flux, quality, and wall superheat. As noted above, to use the post-CHF heat transfer models of TRACE would require the solution of a full two-fluid model and so is impractical for this application. Instead, the film boiling look-up table of Groeneveld et al (2003) was used in this design study.

In this look-up-table, the film boiling heat transfer coefficient is given as a four-dimensional table, however COMSOL-MP only has the capability of performing interpolation for three-dimensional tables. To resolve this, separate 3D tables were generated for each pressure level and imported into the corresponding COMSOL model. An example of the minimum film boiling heat flux calculated using this approach is given below in Figure 6. This value for the minimum film boiling heat flux provides a lower limit for the test section wall heat flux if steady-state film boiling conditions are to be maintained. The film boiling LUT will be used to evaluate the heat transfer coefficient whenever the wall temperature exceeds T_{min}.

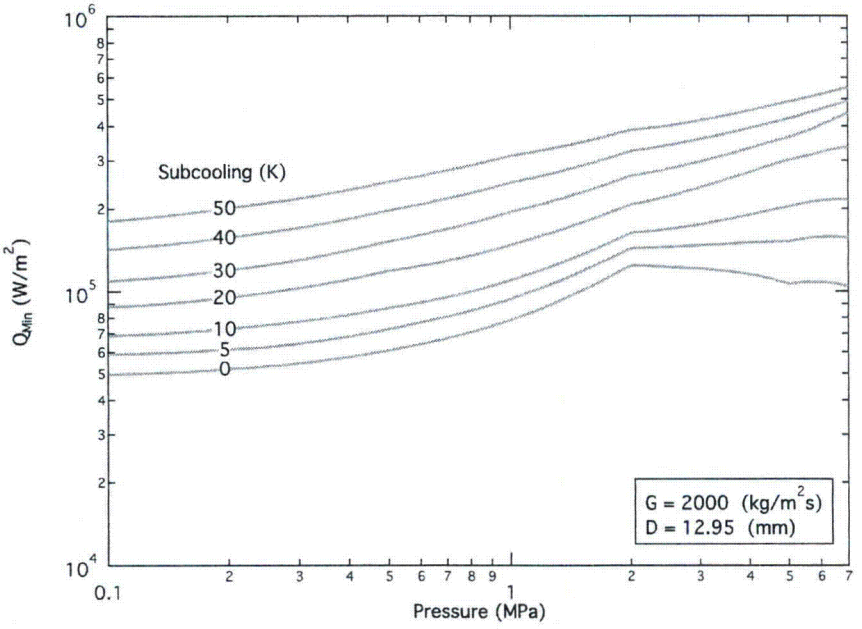

Figure 6: Minimum film boiling heat flux as a function of pressure and subcooling for a mass flux of 2000 (kg/m^{2}s) calculated using the film boiling look-up-table.

Between the CHF and the MFB points, the transition boiling regime provides the transition between the "wet wall" heat transfer of the nucleate boiling regime and the "dry wall" heat transfer of the film boiling regime. The wall heat flux in the transition boiling regime is calculated using the TRACE interpolation scheme as

$$q''_{TB} = f_{wet} \cdot q''_{CHF} + \left(1 - f_{wet}\right) \cdot q''_{min}$$

where

$$f_{wet} = \left(\frac{T_w - T_{CHF}}{T_{min} - T_{CHF}} \right)^2$$

An example of boiling curves calculated during COMSOL simulations using the above models is given in Figure 7. Note that these boiling curves are functions of the local equilibrium quality that varies along the test section during the calculation and so the local subcooling is not fixed. This dependency is responsible for the small bump that

occurs in the film boiling region for the 150 (kg/m^{2}s) curve due to the quality change at the "hot notch".

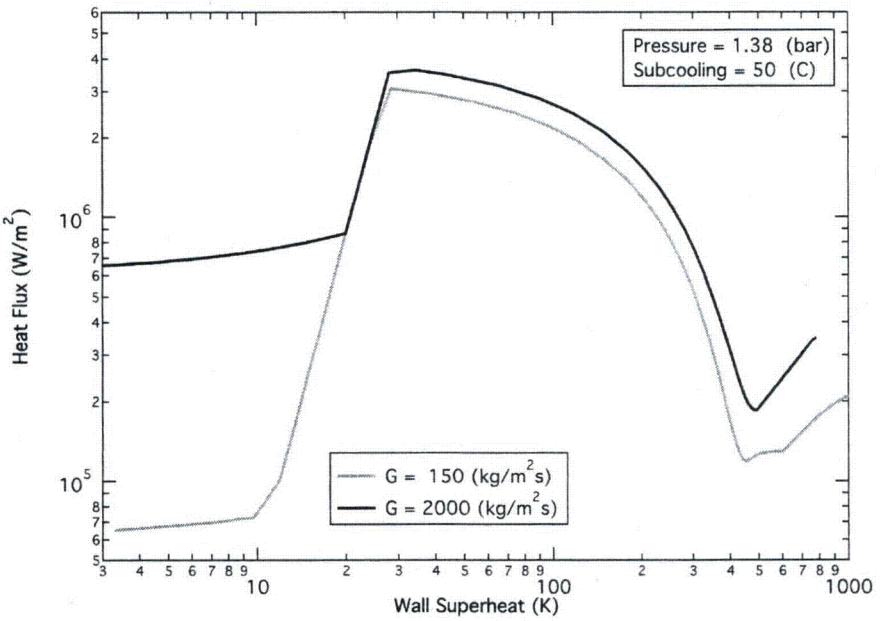

Figure 7: Example of boiling curves calculated during hot patch simulation calculations at a pressure of 1.38 bar (20 psia).

This completes the description of the models used to calculate the boiling curve for this hot patch design study. The next section describes the PID controller that was used to control the hot patch power in order to match the notch temperature to a specified set point value.

Temperature Controller

Because of the non-linearity intrinsic to the boiling curve, it is impossible to do a direct steady-state calculation, so a transient simulation is required for this hot patch simulation study. Also, it is impossible to know a priori the correct power level for the bottom hot patch necessary to stabilize the quench front for the selected flow conditions (pressure, mass flux and subcooling). Consequently, to automatically find the correct hot patch power level during these transient simulations, a proportional-integral-derivative (PID) controller was implemented.

For these simulation studies, the hot patch power refers to the power applied across the bottom set of power terminals, which is section AB of Figure 3. The objective is to control the hot patch power so that the quench front is stabilized but without inducing unnecessarily high temperatures in the high-powered notch region. As noted above, the average wall heat flux for the notch region is about double that of the hot patch region as a whole and so proper power control is necessary to prevent overheating and possible failure. The PID control algorithm used to calculate the hot patch power, P_{HP}, is

$$P_{HP} = k_P \cdot (T_{set} - T_N) + k_I \cdot \int_0^t (T_{set} - T_N) \cdot dt + k_D \cdot \frac{\partial}{\partial t}(T_{set} - T_N)$$

where

k_P, k_I, k_D : control parameters for proportional, integral and derivative

t : time (s)

T_N : notch temperature (°K), measured on outside surface at midpoint

T_{set} : set point for notch temperature (°K)

In practice, the derivative constant, k_D, was set to zero as the appropriate value for this parameter can be difficult to determine and the derivative term may increase the fluctuations in the system because it tends to amplify noise in the error $T_{set} - T_N$.

Reasonable values for the proportional and integral control parameters were determined through trial and error to be:

$$k_P = 5 \quad (W/K)$$

$$k_I = 10 \quad (W/K \cdot s)$$

with a notch set point temperature of 800 °K.

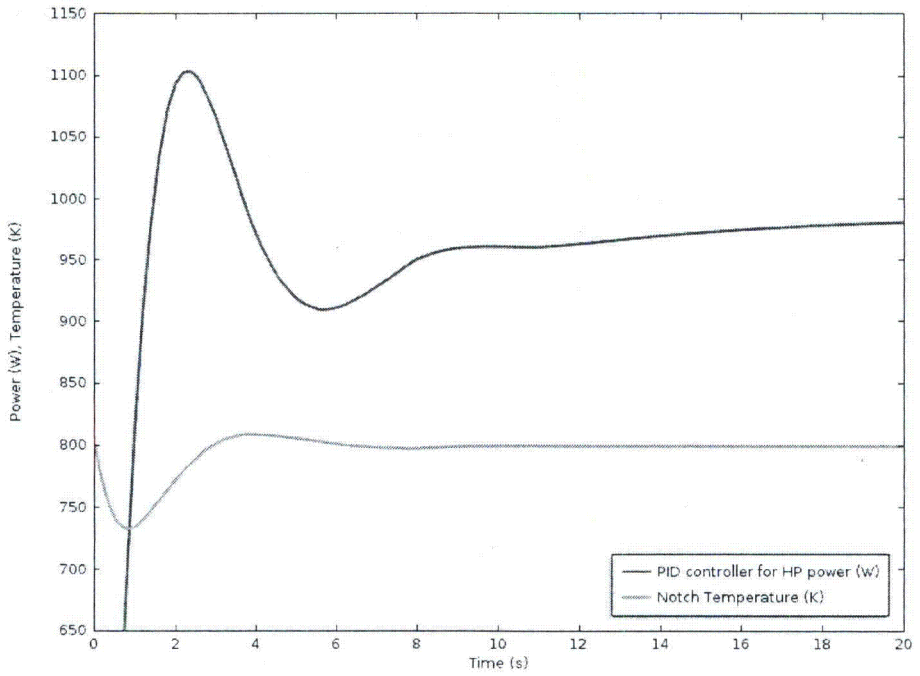

Figure 8: Close-up of PID controller results for base case simulation.

An example of the efficacy of this temperature-power controller is given in Figure 8 that shows a close-up of both the controlled hot patch power and the resulting notch

temperature versus time for the first 20 seconds of the transient. Initially the hot patch power was set to zero and rose almost linearly to a value of 1100 W in 2.4 seconds before converging to its final value of 999.1 W. The notch temperature was initialized at its set point value of 800 °K and fell to a minimum of 734 °K. The maximum notch mid-point temperature encountered during this simulation was only 808.5 °K.

Initial & Boundary Conditions

For the transient hot patch simulation studies described below both initial and boundary conditions must be specified. The initial conditions are simply an axial temperature profile for the following three regions:

Test Section	:	1000 (°K)
Hot Notch	:	800 (°K)
Pre-Heater	:	inlet temperature

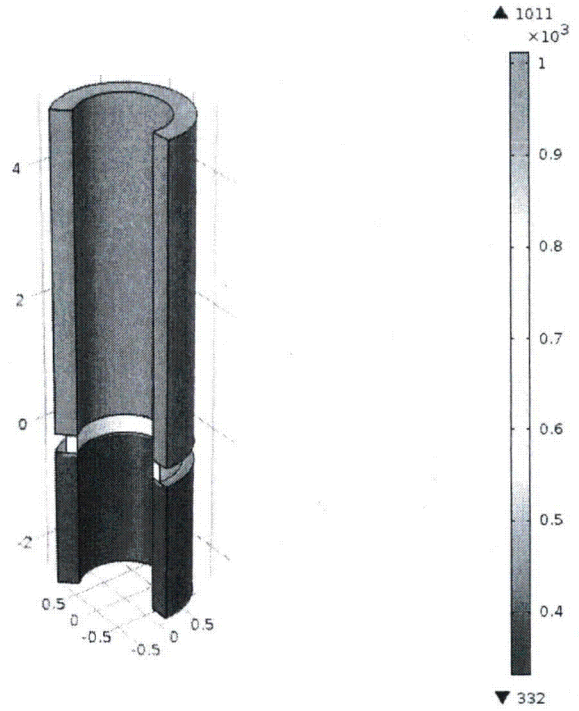

Figure 9: Initial temperature distribution for hot patch simulation studies.

The bottom hot patch is composed of two regions: the "hot notch" itself, and a pre-heater section. The entire notch region is initialized to the notch set point temperature while the pre-heater region is set to the fluid inlet temperature. This allows for the quench front to initially form at the bottom of the notch and greatly facilitates the transient. Otherwise, if the temperature of the pre-heater region was in the film boiling regime, the quench front would form at the inlet and a reflood transient would ensue as it progresses upwards to its final position just below the notch. In practice, this reflood transient is what would be expected to occur during an actual experiment.

The test section is the powered region between the bottom notch and the top notch. For purposes of these simulations, only the first five centimeters of the test section was modeled to reduce computational times. For steady-state film boiling tests with water as a coolant it is necessary to initialize the test section temperature significantly above the minimum film boiling temperature to prevent its quenching at the onset of the transient. This is true both for the numerical simulations described here and for the actual experiments as the power required to initiate dryout would be excessive and might lead to material damage due to over-heating of the notch. Here the initial test section temperature is simply set to a constant value of 1000 K.

Boundary conditions include both those for the fluid and the heat transfer solutions. For the fluid, the mass flux, subcooling and pressure are specified in order to determine the axial profile of the equilibrium quality and the wall heat transfer coefficient including both the CHF and MFB points. For the tube wall, the outer surface is considered to be perfectly insulated, as is the upper boundary. In practice both the insulating material and the heat losses would need to be modeled. At the bottom boundary of the tube wall, the temperature is held at the value of the fluid inlet. Again, for a true pre-test calculation, it would be necessary to model some portion of the unheated section below the pre-heater region.

The power applied to the test section is set to a value corresponding to the desired heat flux operating condition and held constant. As noted above, this value needs to be at least somewhat above the minimum film boiling heat flux in order to prevent spontaneous quenching of the test section. The maximum heat flux value is primarily limited by test section temperature considerations though it can also adversely affect the ability of the PID controller to stabilize the quench front. The hot patch power, that includes both the notch and pre-heater regions, is controlled as described above to keep the notch mid-point temperature at its set point value.

Sensitivity Studies

To help finalize a reasonable hot patch design, a series of sensitivity studies were conducted looking at the effect of hot patch power, the notch length and depth, the test section heat flux, and the system pressure. Before describing these sensitivity studies, the results of the "base case" for the final design will be detailed.

Base Case

The flow conditions selected for the base case were as follow:

Pressure	:	1.379 (bar) [20 psia]
Mass Flux	:	2000 (kg/m^2s)
Subcooling	:	50 (°K)
Heat Flux	:	250 (kW/m^2)

The pressure was set to the minimum value used in the RBHT experiments as low pressure correlates with low heat transfer coefficients and hence high notch temperatures. Conversely, the mass flux was set to the maximum value expected to be run in the experimental program as that corresponds to higher values of the critical heat flux and hence higher hot patch power requirements. Inlet subcooling was specified as 50 °K as that is about the maximum practical value. Although higher values of the

subcooling would be desirable for the experimental program, its effect upon the minimum film boiling temperature, see Figure 5, may render this impractical as for these conditions T_{min} increases about 6.3 °K for every degree of subcooling. Finally, the test section wall heat flux was taken as 250 (kW/m^2) so that it would be about 1/3rd greater than that of the MFB point.

As discussed above the hot patch power was controlled so that the outside wall temperature at the notch mid-point would match its set point value of 800 °K. This required a hot patch power of 999.1 W and yielded a maximum notch temperature of 882.9 °K. Figure 10 shows the calculated temperature profile for the base case conditions where it can be seen that most of the axial temperature gradient occurs across the notch.

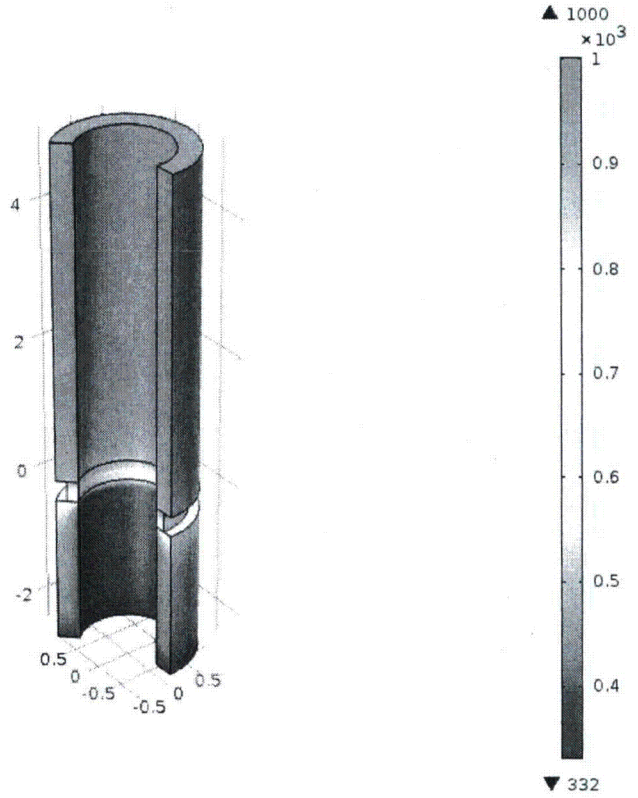

Figure 10: Calculated 3-D temperature profile for base case conditions.

The stabilization of the quench front at the notch region is further delineated by the axial prolife plots of Figure 11 and Figure 12 where the notch is located between the 0 and the -0.3 cm elevations. For these conditions T_{min} is about 879 °K which is just slightly greater than the tube inside wall temperature of 867.5 °K at the top of the notch. Also, as shown in Figure 12, the minimum wall heat flux point also coincides with the top of the notch. The maximum heat flux point, that is the CHF point, is located at about the -0.42 cm position and so is in the pre-heater region just slightly more than 1 mm below the notch.

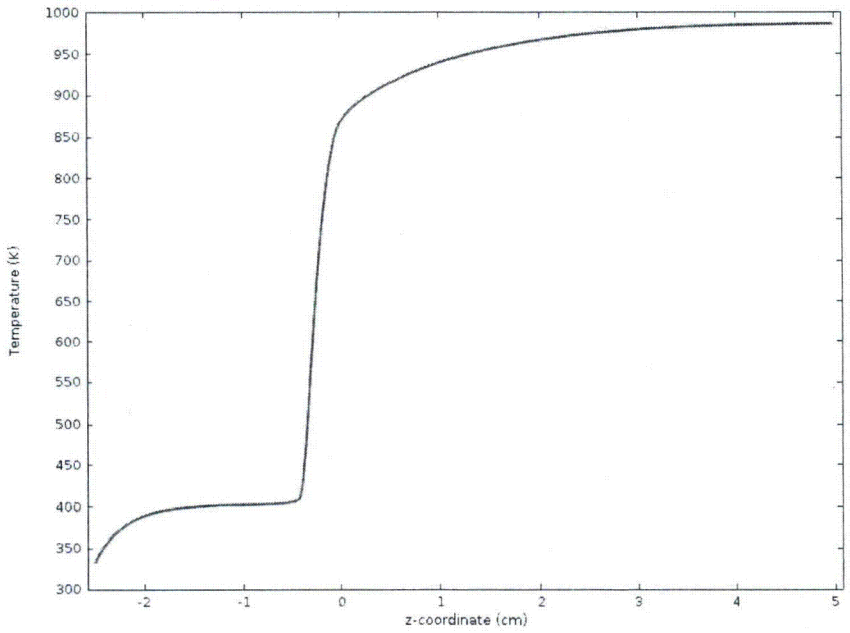

Figure 11: Axial profile of the tube inside wall temperature for the base case showing location of the stabilized quench front in the notch region (from 0 to -0.3 cm).

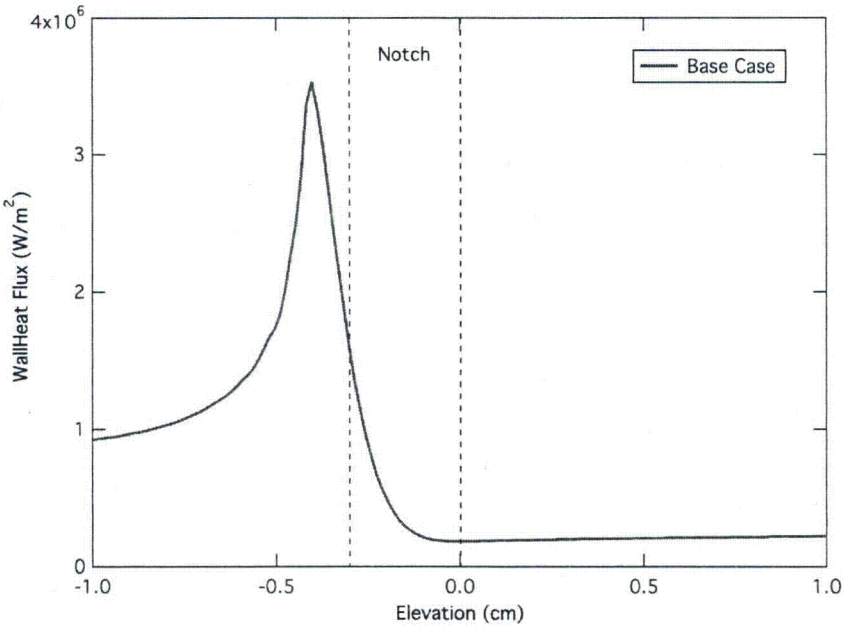

Figure 12: Close-up of the axial heat flux profile for the base case showing the location of the stabilized quench front relative to the "hot notch".

This completes the description of the simulation results for the base case; the remainder of this section presents the results of the various sensitivity studies that helped select the hot patch design parameters.

Hot Patch Power

The hot patch power necessary to stabilize the quench front is a result of the notch geometry, the flow conditions and the test section heat flux. Using the PID power controller to force the notch mid-point temperature to its set point value effectively removes the hot patch power as a sensitivity parameter. However, one of the most important features of the design is the size of the possible operating range for the hot patch power. Consequently, with the PID controller turned off, a sensitivity study was performed to determine the minimum and maximum hot patch powers that would result in a stabilized quench front for the flow and test section heat flux conditions of the base case.

For the purposes of these sensitivity studies, the allowable operating range was determined to the nearest watt and steady-state film boiling conditions were considered to be achieved when time derivative of the notch temperature was less than 0.1 (°K/s). The minimum power condition is that just sufficient to keep the test section from quenching (advancing quench front), while conversely the maximum power condition is that just below a value that would cause dryout of the pre-heater section (receding quench front).

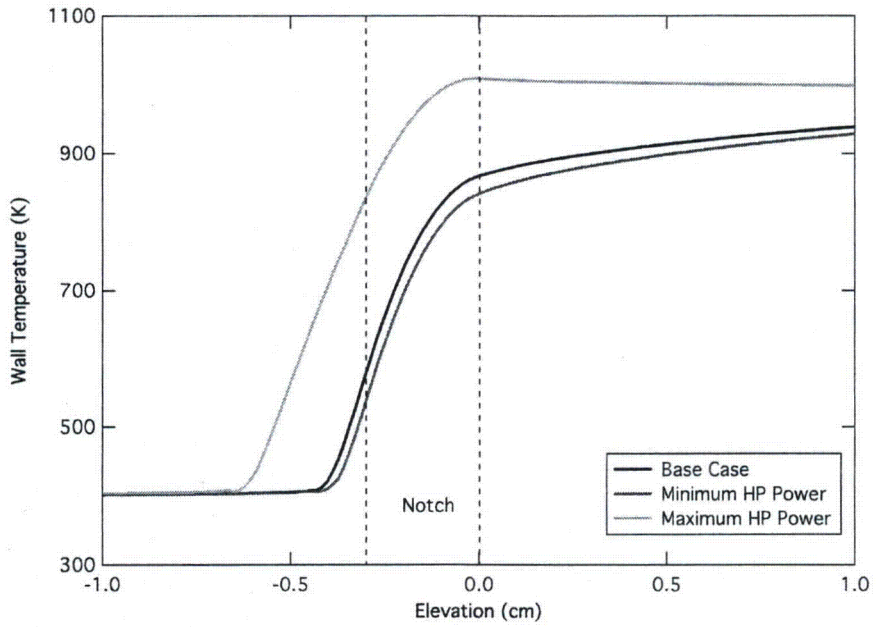

Figure 13: Comparison of tube inside wall temperature profiles in the notch region for the possible hot patch operating power range at the base case conditions.

A comparison of the tube axial temperature profiles for the notch region is given in Figure 13 for the entire possible hot patch power operating range. The operating power levels

and resulting temperatures of interest are given quantitatively in the table below. Here we see that the PID controlled case is only slightly above the minimum power condition and so provides a well-stabilized quench front but without undue high-temperature conditions for the thin-walled notch region. As the hot patch power is increased to its maximum operating point, the quench front recedes further into the pre-heater section and the peak temperature location can move from the test section into the notch region with possible negative consequences relative to structural integrity.

Sensitivity Case	Hot Patch Power (W)	Notch Temperatures[3] (°K)	
		Mid-Point	Maximum
Base (PID Controlled)	999.1	800	882.9
Minimum HP Power	987	770.7	858.2
Maximum HP Power	1102	974.9	1017.7

The crucial result from this sensitivity study is the size of the possible operating envelope for the hot patch power. This is crucial due to its effect upon the controllability of the hot patch power itself. A narrow operating envelope would require precision control and be susceptible to small fluctuations in the flow conditions, whereas a large operating envelope would be easier to control and more forgiving. The envelope for this base case design has a relatively large operating envelope where the power can vary by as much as 115 (W).

One other result of this sensitivity study is the necessity of powering the bottom hot patch separately from the film boiling test section. For example, for the base case discussed above, the heat flux in the film boiling region is 250 (kW/m^2) whereas in the pre-heater region below the notch, the applied wall heat flux due to the hot patch power would be 860.9 (kW/m^2). This is a factor of 3.44 times greater and would require a current 1.86 times as large as that of the test section.

Notch Length

The most critical design parameter was determined to be the notch length. For this study, the notch length was varied ±1 mm from its base design value of 3 mm and comparisons made based on the hot patch operating range and notch maximum temperature. The hot patch operating range was defined as the difference between the minimum and maximum values of the hot patch power for which the quench front can be stabilized. At hot patch powers lower than the operating range, the test section will quench no matter that the applied heat flux is greater than the MFB point. Conversely, for hot patch powers higher than the operating range, the tube will dryout as the quench front recedes into the pre-heater section. The maximum notch temperature is simply that, the maximum value for the material temperature in the notch region and is

[3] In this and subsequent tables, the notch temperatures correspond to those of the outside surface.

important due to its effect on the mechanical strength of this thin-walled region where the highest stresses will occur.

The results of the notch length sensitivity studies are given in the following table:

Sensitivity Case		Hot Patch Power (W)	Notch Temperatures (°K)	
			Mid-Point	Maximum
Base Case (ΔZ_N = 3 mm)	Min. HP Power	987	770.7	858.2
	PID Controlled	999.1	800	882.9
	Max. HP Power	1102	974.9	1017.7
Short Notch (ΔZ_N = 2 mm)	Min. HP Power	1221	808.9	865.8
	PID Controlled	-	-	-
	Max. HP Power	1235	885.6	928.8
Long Notch (ΔZ_N = 4 mm)	Min. HP Power	853	776.2	886.2
	PID Controlled	859.8	800	903.6
	Max. HP Power	1025	1038.3	1081.3

For each sensitivity case, results from three separate calculations are presented in the above table: the PID controlled power case, and the minimum and maximum hot patch power calculations. This both defines the possible hot patch operating range but also gives some perspective on the performance the PID controller. The base case has a notch length of 3 mm and provides for flexible hot patch power control due to a relatively wide operating range of 115 (W). Note also that the PID controlled case is only slightly above the minimum power case and so, at least for these flow conditions, the selection of 800 °K as the set point provides for stable operation without unnecessarily high notch temperatures.

Decreasing the notch length to 2 mm, which is still longer than that used by Winfrith, increases the hot patch power by more than 20% and drastically reduces the operating range. With this shorter hot patch, operation with a stabilized quench front was only found to be possible within a power range of 14 (W). Such a narrow operating range would make the hot patch power control very difficult and sensitive to very small fluctuations in the flow conditions. Indeed, it was not possible to use the PID controller with a set point of 800 °K for the notch mid-point temperature as this temperature was already exceeded for the minimum power condition. For the Winfrith Series 5 tests, the temperature of the bottom hot patch was reported and ranged from 1000-1100 °K which was about 200 °K hotter than the film boiling region of the test section itself. It is possible that the need to run at such high notch temperatures, likely due to the short 1.5 mm length of the notch, resulted in the relatively short working life reported for their test section.

Increasing the notch length to 4 mm further increased the hot patch power operating range to 172 (W) while also further decreasing the hot patch power. However, as the notch length increased, more of the notch region was exposed to film boiling and so a small increase in its maximum temperature was observed for the PID controlled case. For the maximum power case, the entire notch region was in the film boiling heat transfer regime and this, coupled with the high hot patch power, caused the peak temperature to occur in the notch region, as shown in Figure 14. Consequently, even though the possible operating range is larger than that of the base case, much of this extended range would be at the expense of higher notch temperatures and so would be best avoided.

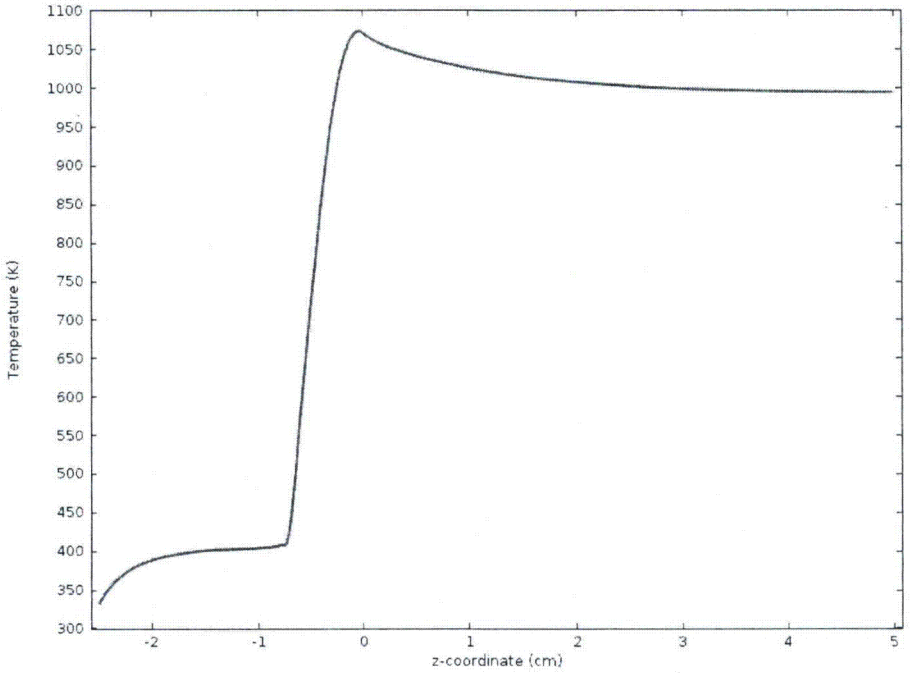

Figure 14: Axial profile of the tube inside wall temperature for the maximum hot patch power case with a notch length of 4 mm.

The above together with the desire to keep the notch length as small as possible to better localize the quench front led to the selection of 3 mm for the notch length corresponding to an operating range of 115 (W).

Notch Depth

The notch depth controls the level of the heat generation spike at the notch region and hence the deeper the notch, the lower the required hot patch power. However, increasing the notch depth, obviously, reduces the wall thickness and so adversely affects the structural integrity of the test section. For this sensitivity study, the notch depth was varied ±0.1 mm from its base design value of 1.5 mm resulting in the following values for the linear heat rate ratio and the hoop stress geometry factor:

Sensitivity Case	$\left(q'_N / q'_{PH}\right)$	$\left(D_I / 2 \cdot \delta\right)$
Shallow Notch (δ_N = 1.4 mm)	2.03	3.93
Base Case (δ_N = 1.5 mm)	2.17	4.18
Deep Notch (δ_N = 1.6 mm)	2.38	4.47

In this sensitivity study, the notch depth exhibited the same trends on operating range, hot patch power and maximum notch temperature, as did the notch length. Specifically, the operating range increased from a value of 67 (W) for a notch depth of 1.4 mm to a value of 153 (W) for a depth of 1.6 mm. Also, though the hot patch power requirements decrease with notch depth, the resulting increases in the notch heat generation rate result in somewhat higher temperatures as shown in the following table:

Sensitivity Case		Hot Patch Power (W)	Notch Temperatures (°K)	
			Mid-Point	Maximum
Base Case (depth = 1.5 mm)	Min. HP Power	987	770.7	858.2
	PID Controlled	999.1	800	882.9
	Max. HP Power	1102	974.9	1017.7
Shallow Notch (depth = 1.4 mm)	Min. HP Power	1053	796.4	875.1
	PID Controlled	1054.3	800	877.9
	Max. HP Power	1120	940.8	987.8
Deep Notch (depth = 1.6 mm)	Min. HP Power	926	775.8	867.0
	PID Controlled	941.4	800	886.4
	Max. HP Power	1076	989.0	1031.6

Based on these results, to keep the hoop stress geometry factor as low as possible yet maximize the operating range, an intermediate value of 1.5 mm was selected for the notch depth.

Test Section Heat Flux

To operate stably in the film boiling region, in addition to a correctly working hot patch, the applied heat flux for the test section must be greater than that of the minimum film boiling point. If the test section power were reduced so that the wall heat flux falls below q''_{min}, spontaneous vapor film collapse would occur leading to rapid quenching of the test section. Indeed, this is exactly the experimental procedure used by Stewart & Groeneveld (1981) to determine the minimum film boiling temperature. Consequently, the test section heat flux becomes an important parameter when trying to conduct steady-state film boiling tests.

For the flow conditions chosen for the base case, the value of the minimum film boiling heat flux is about 188.8 (kW/m^2) as shown in Figure 6 above. A test section heat flux value of 250 (kW/m^2) was selected for the base case, so that it would exceed the minimum value by about $1/3^{rd}$ as described above. In this sensitivity study, the heat flux was varied from 200 to 300 (kW/m^2), or roughly from 6% to 60% above the q''_{min} value. The results are given in the following table:

Test Section Heat Flux (kW/m^2)	Hot Patch Power (W)	Temperature (°K)	
		Notch Maximum	Test Section Maximum
200	1083.4	863.5	903.8
225	1039.6	873.0	949.0
250 (Base Case)	998.9	882.0	992.4
275	958.5	890.9	1034.6
300	919.0	899.6	1075.2

As expected, as the test section heat flux increases it becomes easier to stabilize the quench front and the required hot patch power decreases. Also, as expected, the maximum wall temperature[4] in the film boiling region increases as the heat flux is increased. It was also observed that, despite the reduced hot patch power, the maximum notch temperature increases with the test section heat flux. The reason for this increase becomes apparent in Figure 15 where it can be seen that the higher test section wall temperatures affect the temperature at the top of the notch. Note that almost no difference is observed in the axial temperature profiles for the nucleate and transition boiling regimes due to the high heat transfer coefficients there.

[4] The length of the test section used in these sensitivity calculations was only 10 cm. Maximum wall temperatures in the film boiling region would be different in an actual experiment as the quality increases with axial distance.

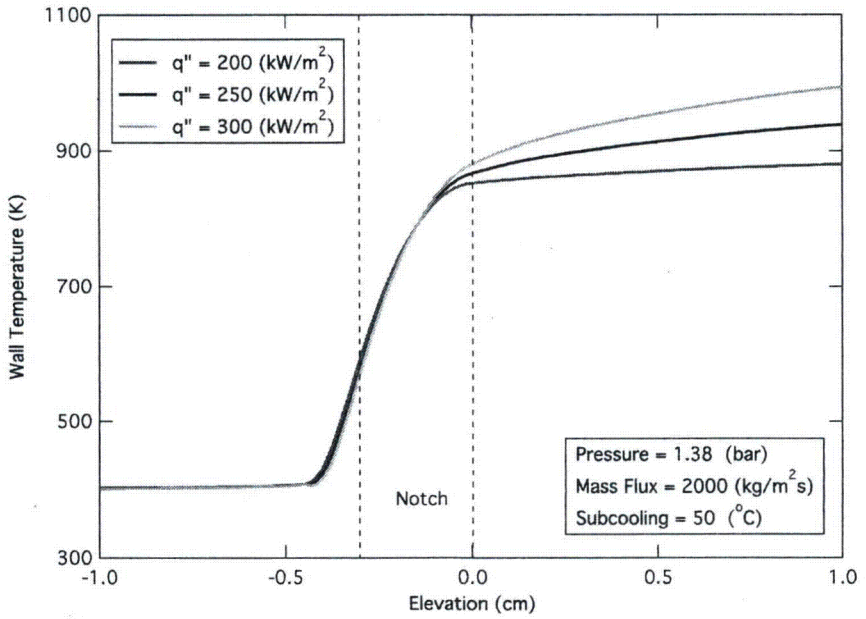

Figure 15: Axial temperature profiles in notch region for base flow conditions with test section heat flux as a parameter.

System Pressure

The last sensitivity study to be conducted was that for the effect of system pressure. The purpose of this study was simply to confirm the operability of the hot patch design for the full range of conditions considered for possible future experimental programs. Here the pressure was varied from 1.379 bar (20 psia), that matches the lowest value used in the RBHT reflood experiments, to a maximum value of 70 bar that is relevant to BWR stability studies and for PWR blowdown rewet.

It was not possible to solely vary the system pressure in this sensitivity study due to its impact on the minimum film boiling heat flux. As shown in the table below, the calculated MFB heat flux increases by a factor of almost 3 as the pressure increases from 1.38 to 70 bar. Therefore, in order to prevent spontaneous quenching of the test section, the applied wall heat flux in the film boiling region has to similarly increase. For these studies, the applied wall heat flux was set to a value about 1/3rd greater than the MFB point and so was increased from 250 to 730 (kW/m^2).

Using the PID controller with a set point of 800 °K for the notch mid-point temperature, the quench front was predicted to be stabilized at the notch over the entire pressure range. Consequently, given the caveat that the validity of these calculations is only as good as the accuracy of the boiling curve that was used, it appears that low-quality high-pressure steady-state film boiling experiments can be successfully conducted even for high mass flux conditions.

The trends with pressure calculated in this study were pretty much as expected with one notable exception. Namely that as the pressure increased from 10 to 70 bar, the required hot patch power decreased. Looking more closely at the details of the boiling curve for these two pressures, one sees that as the pressure increased from 10 to 70

bar, the value of the critical heat flux decreased by about 12%, and that the minimum film boiling temperature decreased from 863.8 °K to 829.8 °K. These decreases serve to explain the lower hot patch power requirement for the 70 bar case.

The results for the system pressure sensitivity study are given in the following table:

Pressure (bar)	Test Section Heat Flux (kW/m^2)	Minimum Film Boiling (kW/m^2)	Hot Patch Power (W)	Temperature (°K)	
				Notch Maximum	Test Section Maximum
1.379 (20 psia)	250	188.8	998.9	882.0	992.4
4.138 (60 psia)	315	235.7	1048.9	885.8	989.6
10 (145 psia)	415	312.4	1251.8	890.5	972.0
70 (1015 psia)	730	551.9	1118.8	883.8	957.3

Conclusions

A hot patch design has been developed to perform low-quality high-pressure steady-state film boiling experiments with water as a coolant. This design is for a joule-heated tubular test section and employs the so-called directly heated hot patch technique to stabilize the quench front at a small notch machined into the tube exterior. The tube OD is 19.05 mm and its ID is 12.95 mm. Sensitivity studies were conducted to select a notch length of 3 mm and a depth of 1.5 mm. This design has a minimum wall thickness of 1.55 mm that is nearly twice as thick as that of the test sections used by the CIAE and Winfrith and so is expected to be more robust.

This design study showed the feasibility of conducting high-pressure steady-state film boiling experiments even for high mass flux conditions. However, the validity of these calculations is only as good as the accuracy of the boiling curve that was used. Consequently, any future experimental program should not rely entirely on computational results such as those of this study but rather include a task for small prototype testing to optimize the hot patch design for the expected flow conditions. The results of such a prototype test program would then be used to both inform the final test section design and to improve the computational tool so that more accurate pre-test calculations could be made.

The directly heated hot patch technique was shown to work well for a joule heated tubular test section. However, to stabilize the quench front, an independent power supply had to be provided for the bottom hot patch. For some high flow conditions, it may also be necessary to independently power the hot patch at the top of the test

section to prevent top-down quenching. The requirement to independently power the hot patch makes this design very difficult to implement in a heater rod such as would be used for rod bundle experiments.

The calculations presented in this study, and upon which these conclusions are based, only considered a thermal analysis for the hot patch design. Before employing this or a similar design in an actual experimental program, the multi-physics aspect of the design problem should be considered. In particular, a solution for the electrical field should be added to this model to assess the impact on the heat flux profile due to the presence of the electrodes (stainless steel plates of about 1.5 mm thickness welded to the test section). Subsequent calculations could also be performed to examine the stress levels at the notches.

References

Chen Y. & Li, J. (1984), "Subcooled Flow Film Boiling of Water at Atmospheric Pressure," in *Two-phase Flow and Heat Transfer*, X. J. Chen and T. N. Veziroglu, 141-150, Hemisphere Pub. Co., ISBN 0-89116-432-4.

Chen, Y.; Fu, X. & Chen, S.P., (1988), "Experimental and Analytical Study of Inverted Annular Film Boiling of Water", in "Experimental Heat Transfer Fluid Mechanics and Thermodynamics", Elsevier Sci. Publ., pp. 1438-1443 (Shah, R. K. et al eds.).

Chen, Y.; Cheng, P.; Wang, J. & Yang, M. (1989), "Experimental Studies of Subcooled and Low Quality of Film Boiling Heat Transfer of Water in Vertical Tubes at Moderate Pressure," *Proc. 4th Int. Topical Meeting on Nuclear Reactor Thermal-Hydraulics*, Vol. 2, 1106-1110.

Chen, Y. (2011), "Heat Transfer in Film Boiling of Flowing Water," in *Heat Transfer - Theoretical Analysis, Experimental Investigations and Industrial Systems*, Aziz Belmiloudi (Ed.), ISBN: 978-953-307-226-5.

Filonenko, G.K. (1954), "Hydraulic Resistance in Pipes," (in Russian), *Teplonergetika*, 1, 40-44.

Gorenflo, D. (1993), "Pool Boiling," *VDI-Heat Atlas*, Sect. Ha, VDI-Verlag, Dusseldorf, 1993. Obtained from secondary reference: J.G. Collier and J. R. Thome, *Convective Boiling and Condensation*, 3rd Edition, p. 155-158, Oxford University Press, Oxford, 1994.

Gnielinski, V. (1976), "New Equations flow regime Heat and Mass Transfer in Turbulent Pipe and Channel Flow," *Int. Chem. Eng.*, **16**, 359-368.

Groeneveld, D.C. (1974), "Effect of a Heat Flux Spike on the Downstream Dryout Behavior," *J. of Heat Transfer,* **96**(2), 121-125.

Groeneveld, D.C, and Gardiner, S.R.M. (1978), "A Method of Obtaining Flow Film Boiling Data For Subcooled Water," *Int. J. Heat Mass Transfer*, **21**, 664-665.

Groeneveld, D.C., et al (1996), "The 1995 Look-Up Table for Critical heat Flux in Tubes," *Nucl. Eng. Des.*, **163**, 1-23.

Groeneveld, D.C; Leung, L.K.H.; Vasic, A. Z.; Guo, Y.J. & Cheng, S.C. (2003), "A Look-Up Table for Fully- Developed Film Boiling Heat Transfer," *Nucl. Eng. Des.*, **225**, 83-97.

Savage, R.A.; Archer, D. & Swinnerton, D. (1992), "Heat Transfer and Voidage Measurements in Steady State Post-Dryout at Low Quality and High Pressure," IChemE 3rd UK National Heat Transfer Conference, Birmingham.

Savage, R.A.; Archer, D. & Swinnerton, D. (1993), "Flow Visualization, Heat Transfer, and Voidage Measurements in Steady-State Post-Dryout at High Pressure," *Proc. 6th Int. Topical Meeting on Nuclear Reactor Thermal-Hydraulics*, Vol. 2, 1311-1318.

Stewart, J.C. & Groeneveld, D.C. (1981), "Low-Quality and Subcooled Film Boiling of Water at Elevated Pressures," *Nucl. Eng. Des.*, **67**, 259-272.

Swinnerton, D.; Pearson, K.G. & Ralph, J.C. (1988), "Comparison of the Results of Harwell and Winfrith Post-Dryout Experiments," UKAEA Report, AEEW-M-2382.